Sperm Morphogenesis in Wild-type and Fertilization-defective Mutants of *Caenorhabditis elegans*

SAMUEL WARD, YAIR ARGON, and GREGORY A. NELSON

Department of Embryology, Carnegie Institution of Washington, Baltimore, Maryland 21210. Dr. Argon's present address is the Medical Research Council Laboratory of Molecular Biology, Cambridge, CB2 2QH, England. Dr. Nelson's present address is Department of Pathology, Harvard Medical School, Boston, Massachusetts 02115.

ABSTRACT Taking advantage of conditions that allow spermatogenesis in vitro, the timing and sequence of morphological changes leading from the primary spermatocyte to the spermatozoon is described by light and electron microscopy. Together with previous studies, this allows a detailed description of the nuclear, cytoplasmic, and membrane changes occurring during spermatozoan morphogenesis. By comparison with wild type, abnormalities in spermatogenesis leading to aberrant infertile spermatozoa are found in six fertilization-defective (*fer*) mutants. In *fer-1* mutant males, spermatids appear normal, but during spermiogenesis membranous organelles (MO) fail to fuse with the sperm plasma membrane and a short, though motile, pseudopod is formed. In *fer-2*, *fer-3*, and *fer-4* mutants, spermatids accumulate 48-nm tubules around their nuclei where the centriole and an RNA containing perinuclear halo would normally be. In all three mutants, spermatids still activate to spermatozoa with normal fusion of their MOs, but the pseudopods formed are aberrant in most *fer-2* and *fer-4* spermatozoa and in some *fer-3* spermatozoa. In *fer-5* mutant males, spermatozoa do not form. Instead, defective spermatids with crystalline inclusions and abnormal internal laminar membranes accumulate. In *fer-6* mutant males, only a few spermatozoa form and these have defective pseudopods. These spermatozoa retain their fibrous bodies, a structure which normally disassembles in the spermatid. The time of appearance of developmental abnormalities in all of these mutants correlates with the temperature-sensitive periods for development of infertility.

The observation that each of these mutants has a different and discreet set of morphological defects shows that the strict sequence of morphogenetic events that occurs during wild-type spermatogenesis cannot arise because each event is dependent on previous events. Instead, spermatozoa, like bacteriophages, must be formed by multiple independent pathways of morphogenesis.

The development of spermatozoa is among the most intricate examples of cellular differentiation. Detailed morphological studies in many organisms, especially mammals (reviewed in references 13, 33) have raised many questions about the molecular mechanisms controlling cellular morphogenesis. Studies of spermatogenesis in nematodes, which have nonflagellated amoeboid sperm, are less detailed (1, 8, 14, 16, 17, 24, 26, 27, 32, 38), but they raise the same basic problems: how is the morphogenesis of a highly specialized cell controlled and, especially, how is this control specified genetically?

To address these problems, our laboratory has been isolating and analyzing fertilization-defective (*fer*) mutants of the nematode *Caenorhabditis elegans* that have infertile sperm (3, 36). *C. elegans* is an excellent organism for isolation and characterization of developmental mutants (7, 19, reviewed in reference 34). Mutants altered in spermatogenesis or spermiogenesis can be recognized by their sterile phenotype and more than 15 genes that can mutate to alter sperm development have already been identified, (3, 19, 36; L. Edgar, U. Colorado, personal communication; T. Roberts, D. Burke, S. Ward, unpublished observations).

Before mutants can be studied profitably, it is first necessary

THE JOURNAL OF CELL BIOLOGY · VOLUME 91 OCTOBER 1981 26-44

to describe wild-type spermatogenesis. A detailed transmission electron microscopy (TEM) investigation of *C. elegans* spermatogenesis in vivo has been published (38), and we have described spermiogenesis in vitro (30). We show here that the development of spermatids from spermatocytes can also be carried out in vitro. By studying spermatogenesis in vitro and by extending the TEM analysis of in vivo development, we are able to describe the precise sequence of morphogenetic events that generate the mature spermatozoon. We then describe alterations in spermatozoan morphology and alterations in the sequence of morphogenetic events caused by mutations in six different *fer* genes. Comparison of the effect of these mutations enables us to determine the relationships between some of the individual events of morphogenesis.

MATERIALS AND METHODS

Nematode Strains

The wild type is *C. elegans* var. Bristol, strain N2 from Sidney Brenner (Medical Research Council Laboratory of Molecular Biology). The following *fer* mutant strains were isolated in our laboratory (3, 36). They are listed with strain names capitalized, gene names italicized, alleles in parentheses, and linkage groups in Roman numerals (21). BA1: *fer-1*(*hc1*ts)I; BA24: *fer-1*(*hc24*ts)I; BA2: *fer-2*(*hc2*ts)IV; BA3: *fer-3*(*hc3*ts)III; BA4: *fer-4*(*hc4*ts)V; BA23: *fer-5*(*hc23*ts)I; BA6: *fer-6*(*hc6*ts)I. In addition, two strains with mutations, that produce a high incidence of males were commonly used as a source of males, CB1467 (*him-5*[*e1467*]) and CB1490 (*him-5*[*e1490*]). Their sperm have normal fertility (20) and their sperm morphology and motility is indistinguishable from wild type (our unpublished observations). *Him-fer* doubles were used as a source of a male sperm in some experiments: specifically BA524: *fer-1*(*hc1*ts)*him-5*(*e1490*); and BA525: *fer-1*(*hc24*ts)*him-5*(*e1467*).

Worm Growth

Strains were maintained at 16°C on petri plates of agar seeded with *Escherichia coli* strain OP50 as described by Brenner (7). Male strains were maintained by periodic mating. For examination of mutant phenotypes, gravid hermaphrodites were usually transferred to plates at 25°C and allowed to lay eggs for several hours. The ensuing progeny were then examined for the mutant phenotype. For some experiments, larvae, before their temperature-sensitive periods, were transferred to 25°C and examined after maturity.

Hermaphrodites were selected for electron microscope (EM) examination at 50–60 h posthatching when they had already laid a few defective eggs. Males were picked when immature, maintained virgin for 2–3 d and then mated for 3–4 h before fixation. This mating procedure ensures that some spermatozoa are present in the males (28).

Light Microscopy

Adult males were freed of bacteria and dissected with a fragment of razor blade or a fine tungsten needle to release sperm and spermatocytes into a drop of sperm medium (SM): 50 mM HEPES, pH 7.0, 50 mM NaCl, 25 mM KCl, 5 mM $CaCl_2$, 1 mM $MgSO_4$, with either 1 mg/ml bovine serum albumin (BSA) or 10 mg/ml polyvinyl pyrollidone (30). The drop was overlayed with a cover slip supported and sealed with vaseline and sperm were observed with a Zeiss Universal microscope equipped with Nomarski optics and recorded on time-lapse video tape or photographed as described (35). Video tapes were analyzed in real time or speeded up × 9 or × 18.

To identify the meiotic stage of intermediates in spermatogenesis, their DNA content was measured. Cells of various stages were fixed onto BSA-coated slides with Carnoy's fixative, stained with Bisbenzimid H33258 (American Hoechst Corp., Somerville, N. J.) as described by Albertson et al. (2), and viewed with epifluorescence illumination using a Zeiss filter combination 487702. Fluorescence intensity of individual nuclei was measured with a Zeiss microscope photometer PM1 using the smallest aperture that would include the nucleus. Background fluorescence from adjacent regions was subtracted from the readings. When spermatozoa in the same field have a relative fluorescence intensity of 1.0, then primary (1°) spermatocytes have 4.4 ± .03, secondary (2°) spermatocytes 1.8 ± .02, and budding spermatids 1.3 ± .15. This agrees within the limitations of the method with the expected ratios of DNA content, 4:2:1, for these cells, confirming their identification.

Scanning Electron Microscopy

Sperm were dissected from males into SM, or SM without BSA or polyvinyl pyrollidone, on 8-mm circular glass cover slips precoated with 1 mg/ml polylysine. They were fixed by slow addition of Karnovsky's fixative (22) or 1.3% glutaraldehyde in 0.95 SM salts prewarmed at 25°C for 0.5 h at room temperature followed sometimes by overnight fixation at 4°C. Some preparations were postfixed with 1% OsO_4 in 0.08 M phosphate buffer, pH 6.8. These variations made little difference in the appearance of the cells. After fixation, the cells were rinsed with water, dehydrated through graded ethanol, transferred to acetone, then liquid CO_2, and critical point-dried in a Polaron apparatus (Polaron Instruments, Inc., Line Lexington, Pa.). They were then sputter-coated with Au/Pd in a Polaron Sputter Coater, and examined with a JEOL JSM35 scanning electrn microscope equipped with either a Lanthanum hexaboride filament operated at 8 kV or a tungsten filament operated at 15 kV.

Transmission Electron Microscopy

INTACT GONADS: Males and hermaphrodites were usually fixed in 1% OsO_4 in 0.08 M sodium phosphate, pH 7.4, initially at 25°C and then at room temperature for 1 h. They were dissected near the gonad immediately after addition of the fixative. Alternatively, worms were cut in 2% glutaraldehyde in 0.08 M phosphate at 25°C and fixed for 0.5 h, then rinsed and postfixed with OsO_4 as described above. The glutaraldehyde fixation can give better preservation of the sperm cytoplasm, but the fixation varies more than with OsO_4 alone. Specimens were dehydrated, embedded, and sectioned as described in (37). They were sectioned longitudinally so that all developmental stages could be found on a single section. Montages of the entire gonad were assembled from electron micrographs printed at a final magnification of × 10,000–20,000. For each mutant at least three gonads were examined. There was no more variation between individuals than within a single individual worm.

ISOLATED SPERM: Better fixation is obtained when sperm are first released from the worms by dissection. Males were dissected in 2 μl drops of SM salts on polylysine coated tissue-culture dishes maintained at 25°C. After 5–15 min, the sperm were fixed by slow addition of 1.3% glutaraldehyde plus 0.2% tannic acid in 0.95 SM salts prewarmed to 25°C. The tannic acid was added immediately before fixation. After 0.5 h fixation at room temperature, sperm were rinsed, then postfixed for 0.5 h with ice-cold 1% OsO_4 in 0.08 M phosphate, pH 6.8. They were rinsed, dehydrated in graded alcohols, and embedded in EPON 812. After 36–48 h curing at 57°C, the tissue-culture dishes were peeled off, leaving the sperm on the surface of the EPON. Blocks were cured an additional 38–48 h at 70°C and then sperm fields were cut and sectioned. Sections were stained with uranyl acetate and lead citrate and examined with JEOL 100S or Zeiss EM10A electron microscope operated at 80 kV. The effects of other fixation conditions are discussed elsewhere (29). At least two hundred and, in some cases, several thousand sperm were examined for each mutant.

For identification of RNA-containing structures, the histochemical procedure of Bernhard (6) was followed. Cells were fixed in 1.3% glutaraldehyde in 0.95 SM salts, then dehydrated, embedded, and sectioned as described above. Sections on girds were stained for 5 min with 5% uranyl acetate, then treated with 0.2 M EDTA 30 min, washed with water, and stained 1 min with lead citrate. Controls were treated identically except no EDTA was present in the 30-min wash.

All quantitative measurements were made from transmission EM negatives whose magnification was calibrated with a Ladd fine mesh grid (Ladd Research Industries, Inc., Burlington, Vt.). They are reported as mean ± SD.

Terminology

"Spermatogenesis" will mean the entire process of sperm development. The term "sperm" will be used to refer to all haploid male gametes. "Spermatids" will refer to immature haploid cells before activation. "Spermiogenesis" converts spermatids to spermatozoa. "Spermatozoa" will refer to the fully mature gametes which normally have an asymmetric shape, a motile pseudopod, and fused membranous organelles (MO).

RESULTS

Wild-type Spermatogenesis

Spermatocytes are formed in vivo from spermatogonia along the periphery of the testes while each nucleus is in a syncytium with a central cytoplasmic core called the rachis (24, 38). After entering meiosis, primary spermatocytes bud off the rachis. From this stage onward, some spermatocytes will develop in

vitro to form mature spermatids (Fig. 1), allowing determination of the sequence and timing of morphogenesis which is summarized in Fig. 2.

When the 1° spermatocyte divides, the 2° spermatocytes either complete cytokinesis or remain attached, causing two pathways of development. If they remain attached, the two spermatocytes elongate in parallel (Fig. 1 *b* and *c*) while their nuclei complete their second meiotic division. A residual body begins to form between each of the now haploid nuclei. This central body enlarges and coalesces into one, leaving the haploid nuclei at the corners (Fig. 1 *c–h*). The cytoplasmic bridge between the two spermatocytes can twist so that the four nuclei lie in a plane or at the corners of a tetrahedron. If the 2° spermatocytes do separate completely their nuclei divide and segregate as described above with the residual body forming between them.

When the contents of a young adult male gonad are examined immediately after dissection, examples of all of the intermediates described above are found so the two pathways observed in vitro must occur in vivo as well. The relative frequency of in vivo intermediates is shown in Fig. 2 in combination with the timing of steps in development determined in vitro.

About 90 min after the first division in vitro, some of the haploid spermatids bud off the residual body. Most remain attached and arrest their development at this point (Fig. 1 *g* and *h*), perhaps reflecting some deficiency in the in vitro conditions. In vivo, all four spermatids separate from residual body, complete some further maturation, and then arrest their development as spermatids until triggered to form mature spermatozoa by mating.

Wolf et al. (38) have described the formation and maturation of sperm organelles during in vivo spermatogenesis and we have described the rearrangements that occur during in vitro spermiogenesis (30). We have taken advantage of in vitro development to establish the precise sequence of early morphological events and to examine some events in more detail. Our new observations are described here and an overall summary of spermatogenesis is shown in Fig. 5.

When the chromatin of the 1° spermatocyte condenses, the nucleus undergoes karyokinesis with an apparently conventional spindle of microtubules. An early stage of the spindle formation is shown in Fig. 3 *a*. The microtubules in the spermatocyte at this stage are narrower than in other organisms with a diameter of only 19 ± 2 nm. This is true of some other

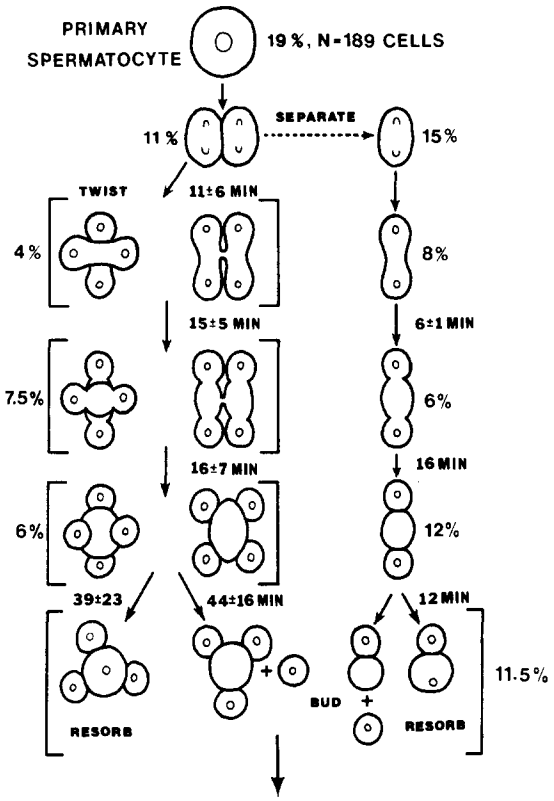

FIGURE 2 Diagram illustrating the two pathways of sperm development. The time between steps is the average interval and SD observed in at least five examples of in vitro development. The percentages show the proportion of intermediates of each class observed immediately after dissection from several males and so reflect the in vivo proportions.

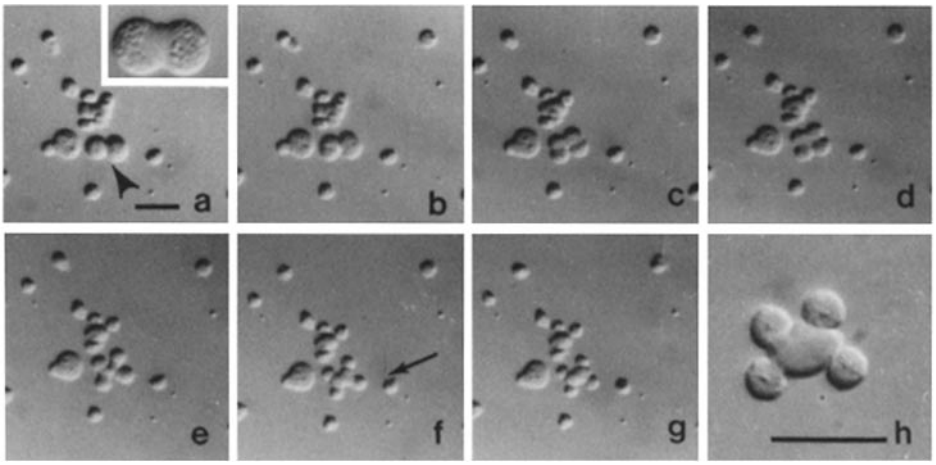

FIGURE 1 Light micrographs of in vitro sperm development. A 1° spermatocyte began to divide at 0 min. *a*, 30 min: arrowhead shows 2° spermatocytes that are developing in this sequence. *Inset* shows similar spermatocytes. *b*, 39 min: 2° spermatocytes are beginning to divide again. *c*, 42 min: haploid nuclei segregating. *d*, 55 min: residual body forming between haploid nuclei. *e*, 69 min: residual body expanding. *f*, 79 min: residual body reaches maximum size. Arrow shows transient filament formed on nearby spermatid. *g*, 120 min. Development has arrested without budding of the spermatids. The filament disappeared from the spermatid nearby. *h* spermatids and residual body. Bars, 10 μm. *a–g*, × 600. h and *Inset*, × 1,500.

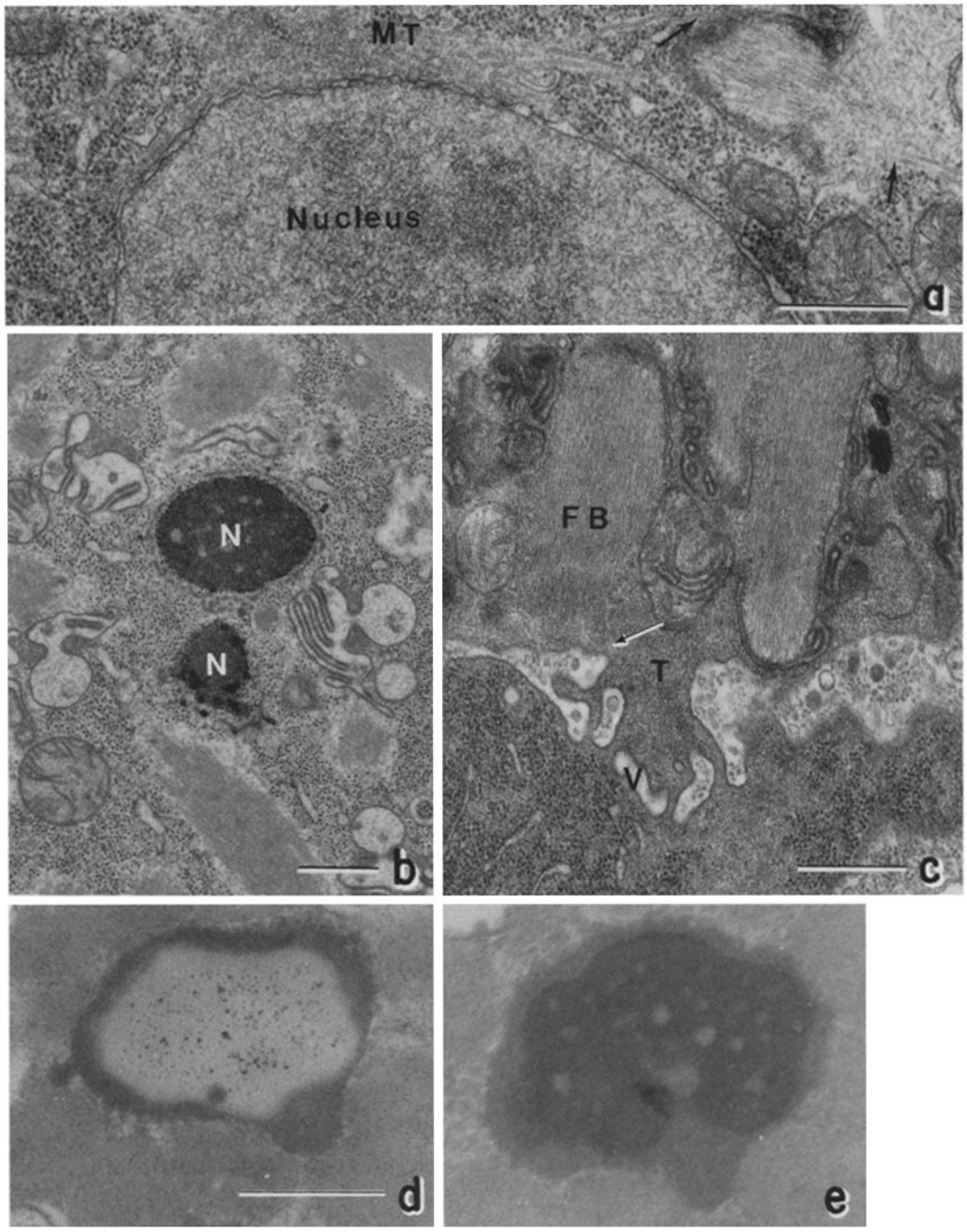

FIGURE 3 TEM of spermatogenesis. *a*, 1° spermatocytes with a forming spindle of microtubules. Arrows show microtubules adjacent to fibrous body (*FB*) MO complex. × 38,000. *b*, nuclei (N) separating in a 2° spermatocyte. Remnants of membrane surround the upper nucleus. No microtubules are found near this nucleus or in other sections of similar nuclei. × 23,000. *c*, spermatid (above) budding off from a residual body (below). Vesicles (V) are found between them. Tubular elements (T) fill the cytoplasmic bridge. The fibrous bodies in the spermatid are oriented with their long axis toward the residual body. × 32,000. *d*, Spermatid nucleus prepared according to Bernhard's procedure. *e*, Control nucleus for d in which the EDTA was omitted from the poststaining treatment. × 42,000. Bar, 0.5 μm.

C. elegans microtubules as well (9). The spermatocyte cortex also contains actin microfilaments that can be decorated with heavy meromyosin (29). These presumably participate in cytokinesis because cytochalasin prevents cleavage furrow formation (29).

It is not apparent how the nuclei segregate at the second meiotic division. The division of the 2° spermatocytes is rapid (2–5 min), so cells at this stage are difficult to find, but no spindle has been observed in dividing 2° spermatocytes that have been sectioned (Fig. 3 *b*). The chromatin does not decondense after the first meiotic prophase, although a nuclear membrane reforms (Fig. 3 *b*). During the final chromatin condensation in the maturing spermatid, an electron-dense perinuclear halo forms that encases the centrosome (38). Examination of cells fixed and stained by Bernhard's procedure suggests that this halo contains RNA, not DNA (Fig. 3 *d* and *e*). This has been claimed for other nematodes (10, 17). A few microtubules are found in the cytoplasm between the residual

body and the poles and the cell (Fig. 3 *c*), but these disappear and are not found in any later stages.

Spermatid budding (in vivo and in vitro) is preceded by formation of membrane vesicles between the spermatid and the residual body. These appear to coalesce to form the membranes separating the spermatids (Fig. 3 *c*). No contractile ring of microfilaments or microtubules can be detected in the constriction at this time in spermatids fixed in vivo or in vitro with a variety of fixatives, and budding is not disrupted by cytochalasins (G. Nelson, unpublished observations). Thus the separation of the spermatid from the residual body appears to resemble plant cell division (31) or the formation of platelet s from a megakaryocyte (40), rather than ordinary animal cell cytokinesis.

Mature spermatozoa are shown in Fig. 4. They are bipolar amoeboid cells with all organelles confined to a hemispherical cell body which is separated from motile pseudopod by the accumulation of laminar membranes (30). Most of the MOs (also called special membrane structures, see reference 38) have fused with the plasma membrane, releasing fibrous material. The pseudopod contains amorphous granular cytoplasm and is devoid of microtubules or microfilaments as is the cell body (29, 30, 38). Fig. 5 summarizes our understanding of the sequence of morphological events during spermatogenesis.

Abnormal Sperm

Even in healthy wild-type males some aberrant spermatozoa are formed. These are usually the oldest sperm in the gonad located in or near the vas deferens. At most, they represent ~5% of the sperm in old males. The morphology of some of these aberrant cells is described here because they are more common in some of the *fer* mutants described below. The most common aberration is for the cells to become even more electron-dense than the normal sperm (Fig. 6 *a*). This is often accompanied by the presence of crystalline inclusions that can span the cell, giving it a skewered appearance. Inclusions are sometimes found in cells which are not electron-dense (Fig. 6 *b*, *c*). When examined in vitro, the most variable features of sperm morphology are the appearance of microspikes and the presence of inclusions. Occasionally, all the spermatids from a male will have inclusions (Fig. 6 *c*); more commonly, only a few cells do. They are sometimes reversible (Fig. 1 *f* and *g*).

Mutant Spermatogenesis

fer-1: When grown at 16°C or 20°C, *fer-1* mutant sperm are indistinguishable from wild-type (3). When grown at 25°C, mutant spermatozoa have a uniform defective phenotype: pseudopods are short and stubby, but they have normal looking projections (Fig. 7 *a*). The average pseudopod length is 1.3 ± 0.35 μm, compared to 2.3 ± 0.29 μm for the wild type. The probability this difference arose by chance is <0.001 (*t* test). Sperm from males with either the *hc1* or *hc24* mutation have similar morphological defects.

Transmission EM examination of sections of *fer-1* mutant spermatozoa confirms the phenotype of short pseudopods with normal projections (Fig. 7 *b*). The spermatozoa have internal

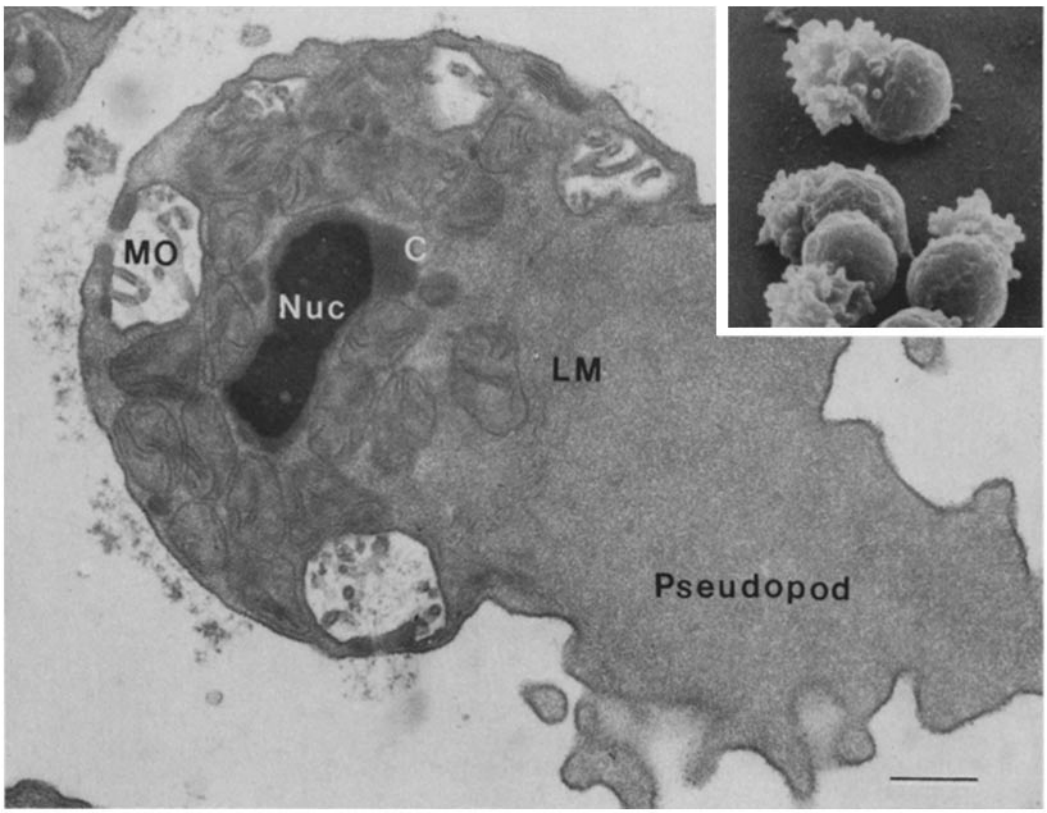

FIGURE 4 Spermatozoa. *Inset* (SEM), four spermatozoa each with an extended pseudopod studded with projections and a rounded cell body. Tilt = 45°. × 5,500. Bar = 2 μm. TEM, mature spermatozoon fixed with GTA and tannic acid, and then OsO_4. Fused MOs can be seen expelling their fibrous contents which remain associated with the cell body surface. Laminar membranes (*LM*) are most pronounced in the region between the cell body. No microtubules or microfilaments are seen in this or thousands of other sections of spermatozoa examined. *NUC*, nucleus, and C, centriole. × 23,000. Bar, 0.5 μm.

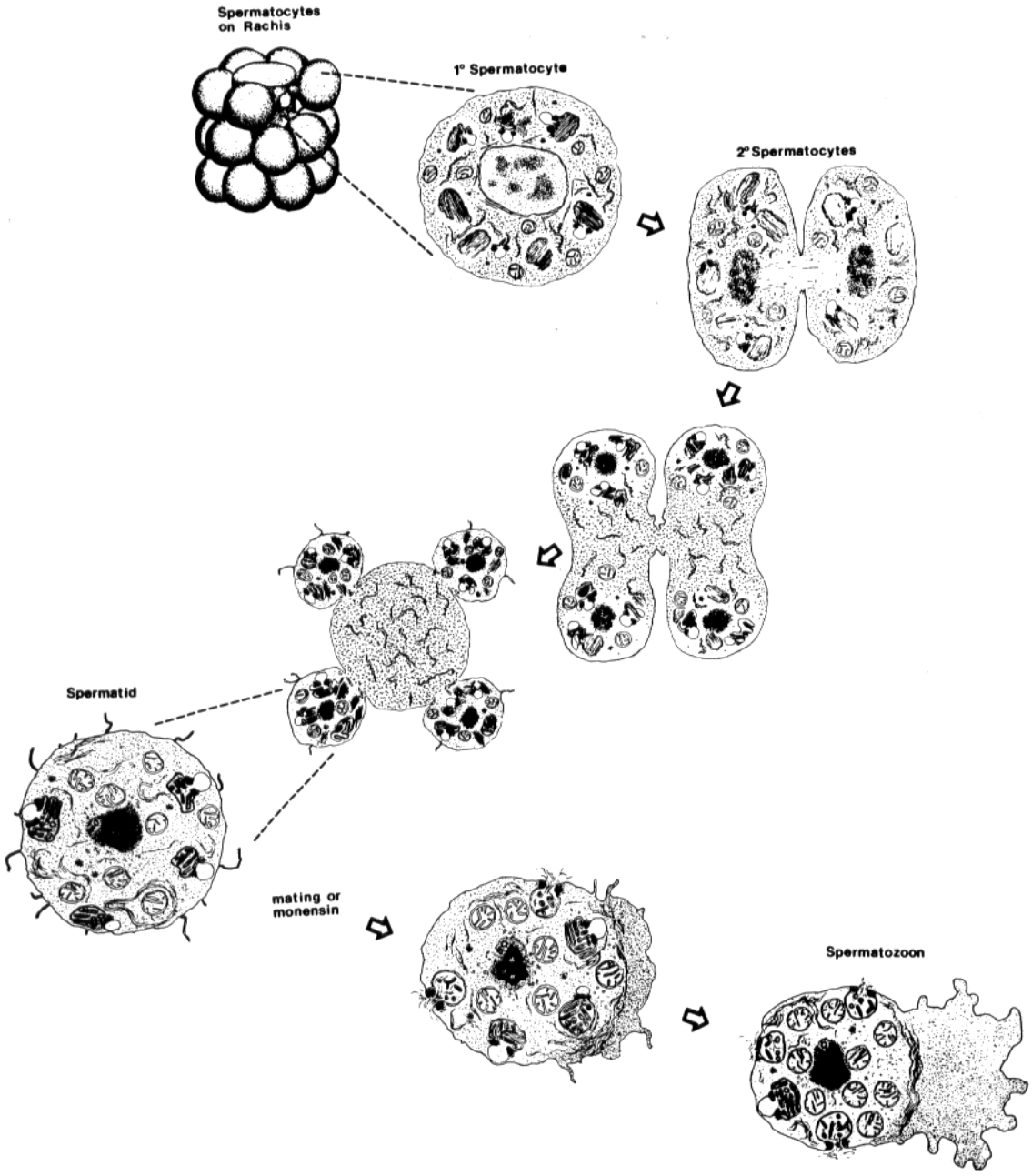

FIGURE 5 Summary of spermatogenesis. See text in discussion.

lamellar membranes concentrated between pseudopod and cell body as in wild type. The MOs, however, fail to fuse with the plasma membrane, although they abut it normally (Fig. 7 *b*, *c*, and *d*). An identical phenotype is found in *fer-1* hermaphrodites (Fig. 7 *e*). The MO-fusion defect is quantified in Table I. In wild-type males grown at 25°C, ~70% of the MOs have fused with the plasma membrane in both male and hermaphrodite spermatozoa. In contrast, no MO fusions have been detected in spermatozoa of either *fer-1* hermaphrodites or males grown at 25°C. Fusions occur normally in the sperm of mutants grown at 16°C (data not shown).

In hermaphrodites, wild-type spermatozoa extend their pseudopods into invaginations in the walls of the spermatheca (35). In contrast, *fer-1* hermaphrodite spermatozoa fail to extend pseudopods into the wall of the spermatheca (Fig. 7 *e*). Instead, the mutant spermatozoa appear to float free in the lumen or just abut the spermatheca. This is also seen when mutant hermaphrodites are examined live with the light microscope. Lack of firm attachment to the spermatheca can explain why these spermatozoa are swept out of the spermatheca by passage of an oocyte (36).

The development of sperm in both *fer-1* mutant males and hermaphrodites is indistinguishable from wild type up to the formation of the mature spermatids which are normal by both scanning and transmission EM. The earlier conclusion that the light microscopic phenotype of *fer-1* mutant sperm was identical to wild type (36) was unwittingly based on comparison of spermatids, not spermatozoa. It is only during the maturation to spermatozoa that the mutant defects in MO fusion and pseudopod extension become evident.

A COMMON DEFECT IN *fer-2*, *fer-3* AND *fer-4*: The spermatozoa from each of these three mutants vary in terminal

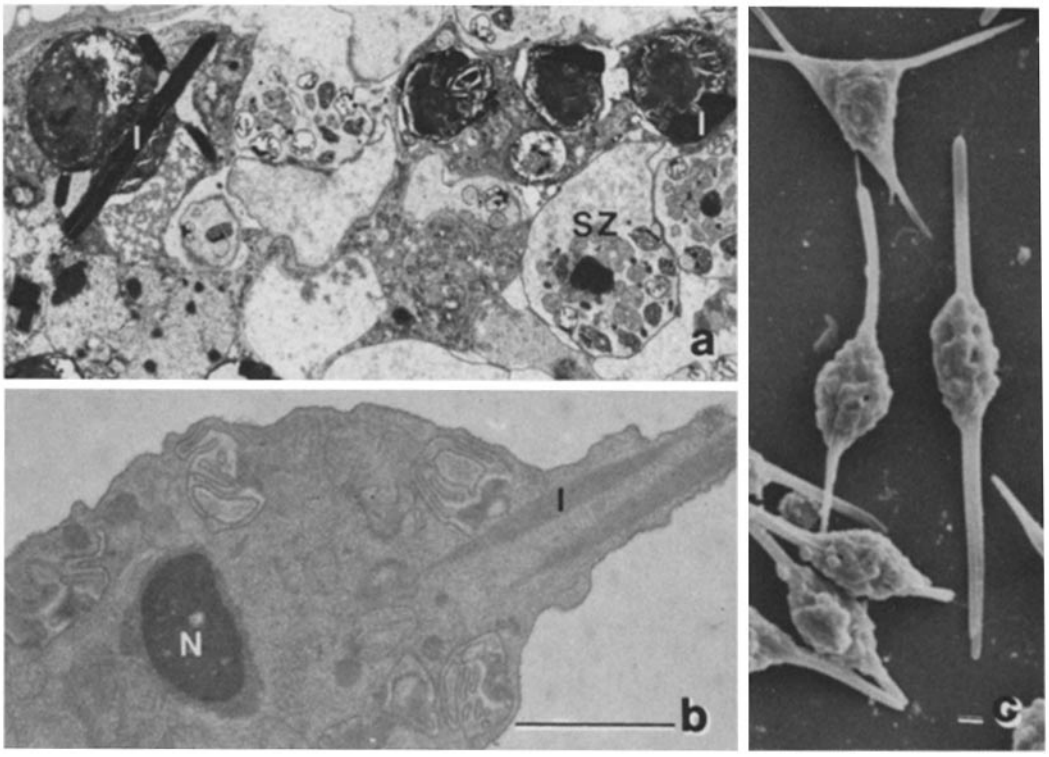

FIGURE 6 Aberrant sperm. *a*, TEM of male seminal receptical near the vas deferens. OsO_4 fixation. A normal spermatozoon is labeled SZ. Four electron-dense aberrant sperm are in a row near the top. Two of these contain crystalline inclusions (I). × 4,200. *b*, a spermatid fixed outside the male with glutaraldehyde then OsO_4. A cytoplasmic inclusion (I) extends from one side of the cell. × 21,000. *c*, SEM of a cluster of spermatids with inclusions from the edge of a field of dissected male sperm. × 3,100. Bars, 1 μm.

morphology more than do the sperm of *fer-1*. They also differ from one another. They are grouped together here because they share one striking morphological abnormality: the accumulation of large tubules around their condensed chromatin. Examples of these tubules are shown in Figs. 8, 10, 12, and 13. They appear as straight hollow cylinders radiating away from the chromatin. This perinuclear region is normally occupied by an amorphous RNA containing material which surrounds the centriole (Fig. 3 *d* and *e*). The amorphous material is missing in all three mutants and the centriole is usually displaced from the nucleus, sometimes by as much as a micron (Figs. 8 *a* and 11 *c*). The diameter of the tubules is 43 ± 7 nm in *fer-4* males, 51 ± 6 nm in *fer-2* males, and 51 ± 8 nm in *fer-3* males. The lengths are hard to estimate from sections, but in *fer-4* males tubules are longer than those in *fer-2* or *fer-3*. The longest *fer-4* mutant sperm tubule in a single section was 1 μm. Tubules do not extend into the pseudopod. The tubules are observed in >90% of sections that include the chromatin in *fer-4* mutant sperm, whereas they are only seen in 60–70% of *fer-2* or *fer-3* mutant sperm sections.

fer-2: Spermatozoa of *fer-2* males grown at 25°C vary in morphology more than those of *fer-1*. They usually have short or nonexistent pseudopods, but sometimes spermatozoa with abnormal multibranched processes are seen (Fig. 9 *a* and *b*). These are often helically twisted. MO fusions occur nearly normally in *fer-2* spermatozoa (Fig. 10 *c* and Table I). Similar morphological defects are found in *fer-2* hermaphrodite sperm as well (not shown).

Filaments are found in the defective pseudopods of some *fer-2* spermatozoa (Fig. 9 *c*). These filaments appear similar to filaments found in *fer-3* pseudopods described below.

Several abnormalities can be detected during *fer-2* mutant spermatogenesis. Sometimes spermatids are found still clinging to residual bodies. This is more common in hermaphrodites than in males. Usually the spermatids bud off normally, but their microspikes are short and less abundant (Fig. 5 *a*). The perinuclear region appears normal in many immature spermatids just after separation from the residual body (Fig. 10 *b*), but it becomes abnormal with large tubules appearing in most of the mature spermatids (Figs. 8 *a* and 10 *c*). In *fer-2* sperm some MOs fail to segregate their fibrous body contents and more MOs fail to abut the plasma membrane in *fer-2* than in wild-type spermatids.

fer-3: The spermatozoa of *fer-3* males grown at 25°C are variable in appearance, but many are normal by SEM (Fig. 11 *a*). The most common defective phenotype is for spermatozoa to have pseudopods which are shorter than wild-type. MO fusion occurs normally in *fer-3* spermatozoa (Fig. 11 *b* and *c*, and Table I).

As in some of the *fer-2* mutant sperm, filamentous material is found in the pseudopods of *fer-3* spermatozoa that are obviously abnormal. Examples are shown in Fig. 6 *c* and *d*. These filaments mingle with the granular material in the pseudopod. Their diameter is 3.6 ± 0.7 nm and the average spacing between them is 2.2 ± 1 nm. In developing spermatocytes and spermatids, filaments of similar diameter are found in the fibrous body (39). In the fibrous body these filaments have a diameter of 4.5 ± 1.1 nm and the spacing between filaments is larger than that found in *fer-3* pseudopods (3.7 ± 1.5 nm). For comparison, muscle actin filaments in tissue in the same sections from which the sperm were measured have a diameter of 6.1 ± 1.4 nm.

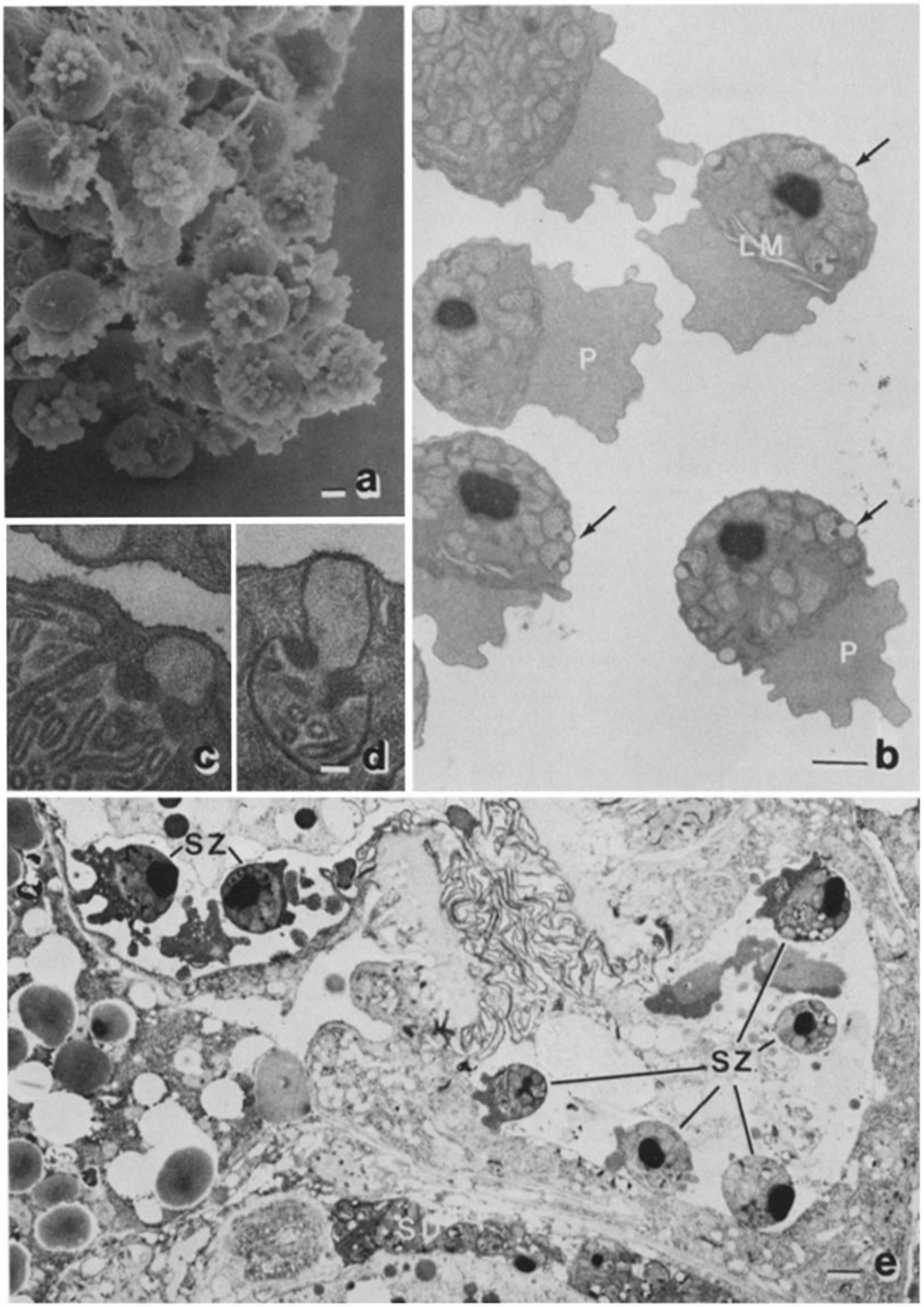

FIGURE 7 *fer-1* spermatozoa. *a*, SEM of a fragment of male seminal vesicle showing many spermatozoa with rounded cell bodies and short pseudopods (*P*) with normal projections. × 3,600. Bar, 1 μm. *b*, TEM of spermatozoa. Laminar membranes (*LM*) separate pseudopods from cell body as in wild type. Arrows show unfused MOs. × 8,200. Bar, 1 μm. c and d, spermatozoa. MOs abutting plasma membrane but not fusing. × 40,000. Bar, 0.1 μm. *e*, hermaphrodite showing five spermatozoa (*SZ*) in spermatheca on the right and two spermatozoa in the uterus on the upper left. OsO_4 fixation. Spermatids (*SD*) are in the oviduct at the bottom. × 5,000. Bar, 1 μm.

Examination of the development of the *fer-3* mutant shows a peculiar condensation of the nucleolus in spermatocytes (Fig. 12*a*). There are also ribosomes in the perinuclear region in some spermatids before budding although others are normal at this stage (Fig. 12*b*, and *c*). The absence of the perinuclear halo and the appearance of large tubules can be seen in the earliest budded spermatids and is found in nearly all mature spermatids (Fig. 12*e*). Most spermatids lack microspikes (Fig. 12*d*). The MOs appear normal and abut the plasma membrane normally in *fer-3* spermatids.

fer-4: *fer-4* mutant spermatozoa have a more uniform appearance than either *fer-2* or *fer-3*. They have normal or slightly long pseudopods (2.8 ± 0.42 μm), but these have only small abnormal projections (Fig. 13*a*). Transmission EM examination reveals that MO fusion occurs nearly normally (Fig. 13*b* and Table I).

TABLE I

MO Fusions in Wild-type and fer Spermatozoa

Genotype	Spermatozoa	Total MO	Fused MO
			%
Wild type ♀	25	108	72
Wild type ♂	122	505	69
fer-1 ♀	48	199	0
(*hc24*) ♂	134	658	0
(*hc1*) ♂	37	165	0
fer-2 ♂	44	185	60
fer-3 ♂	24	136	57
fer-4 ♂	43	226	66

All strains were grown at 25°C. At 16°C, the fraction of MOs fused is ~40% for both wild-type and *fer-1* hermaphrodites. Hermaphrodite sperm were scored from sections of intact hermaphrodite gonads; male sperm from sections of sperm fixed after dissection. Only sperm with pseudopods visible in the plane of section were included to assure that only spermatozoa were scored. All spermatozoa in two or three different fields were scored for each mutant. Data for wild-type males include both N2 and CB1467(*him-5*) males. Data for *fer-1* hermaphrodite indicates both *hc1* and *hc24* hermaphrodites. Fused MOs are readily distinguished from unfused, even in sections that do not include the fusion pore, by their lack of internal electron density, by the reduced number of membrane invaginations and by the presence of their fibrous contents on the cell surface above them. ♀, hermaphrodite; ♂, male.

Analysis of the development of *fer-4* spermatozoa reveals that the large tubules appear in the spermatid before budding (Fig. 12*c*). They are present and the perinuclear halo is absent from all subsequent spermatids (Fig. 12*d*). MO development, alignment, and fusion appear normal.

In *hc4*/+ heterozygotes, spermatozoa bearing the *hc4* mutation are less fertile than + bearing sperm (3). We have examined the sperm of several such heterozygotes with both transmission and scanning EM and can find no spermatozoa with either large tubules, a defective perinuclear halo, or defective pseudopods.

fer-5: *fer-5* male sperm are grossly abnormal in morphology (Fig. 14*a*). A few have pseudopods that are short and aberrant, but most do not. Most *fer-5* sperm are covered with large cavities or collapsed regions and many have large rodlike projections that give the cells a skewered appearance.

Transmission EM examination reveals that there are many intact MOs close against the membrane but few fusions (Fig. 14*b* and *c*). The plasma membrane is often indented toward the MO (Figs. 14*c* and 15*b*) and this contributes to the irregular surface appearance. MO fusion can occur (Fig. 14*c*) in the rare cells with pseudopods.

Crystalline inclusions are commonly found within *fer-5* spermatids and spermatozoa (Fig. 14*b* and *c*). These can sometimes be several times the length of the cells and cause the skewered appearance. These inclusions appear similar to those in old wild-type cells (Fig. 6). They are also found in several other mutants when old males are sectioned. In *fer-5* however, they are more common than in wild type, being found in as many as 25% of the sperm from some males. In spite of the inclusions, the rare spermatozoa still attempt to form a pseudopod (Fig. 14*c*).

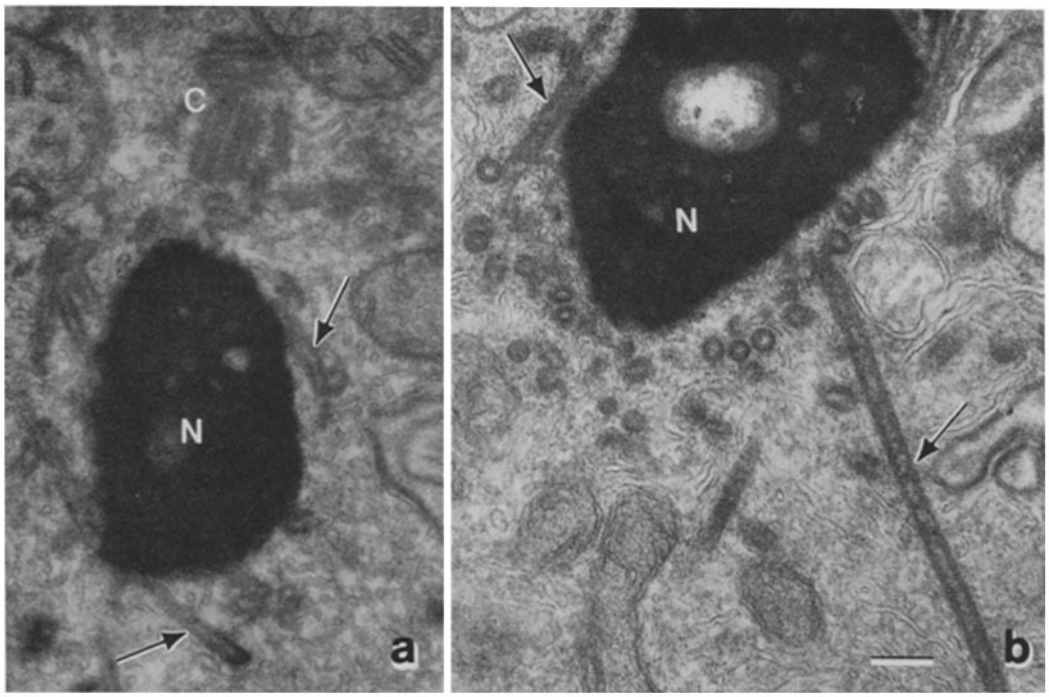

FIGURE 8 Perinuclear tubules. Arrows show large tubules around the nucleus (*N*) in place of the perinuclear halo. *a*, *fer-2*. Spermatozoa with centriole (*C*). *b*, *fer-4*. Spermatozoa. Bar, 0.1 μm. × 80,000.

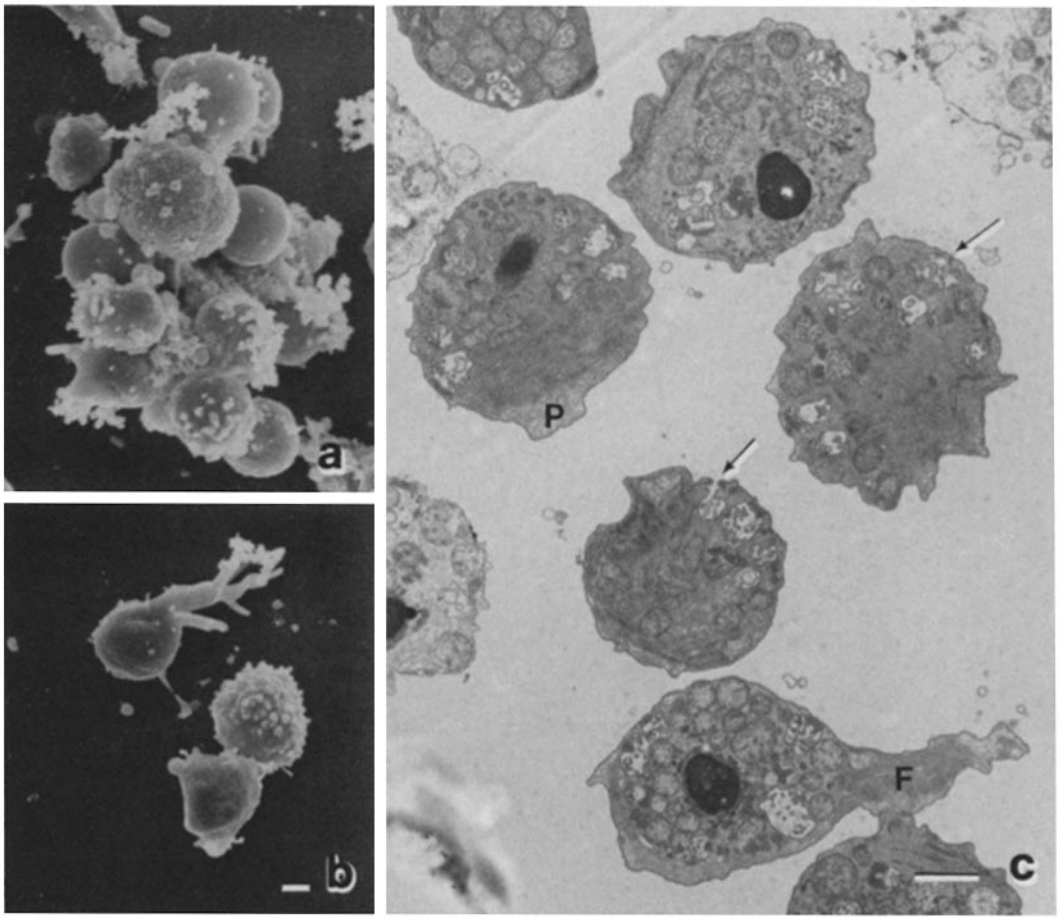

FIGURE 9 *fer-2* spermatozoa. *a* and b, SEM of spermatozoa. *a*, shows a cluster of sperm; spermatozoa have short or aberrant pseudopods with projections; spermatids are smooth with few microspikes. × 3,600. *c*, TEM of spermatozoa, some with aberrant pseudopods (*P*). Fibrous elements (*F*) are found in one pseudopod. Arrows show fused MOs. × 8,200. Bar, 1 μm.

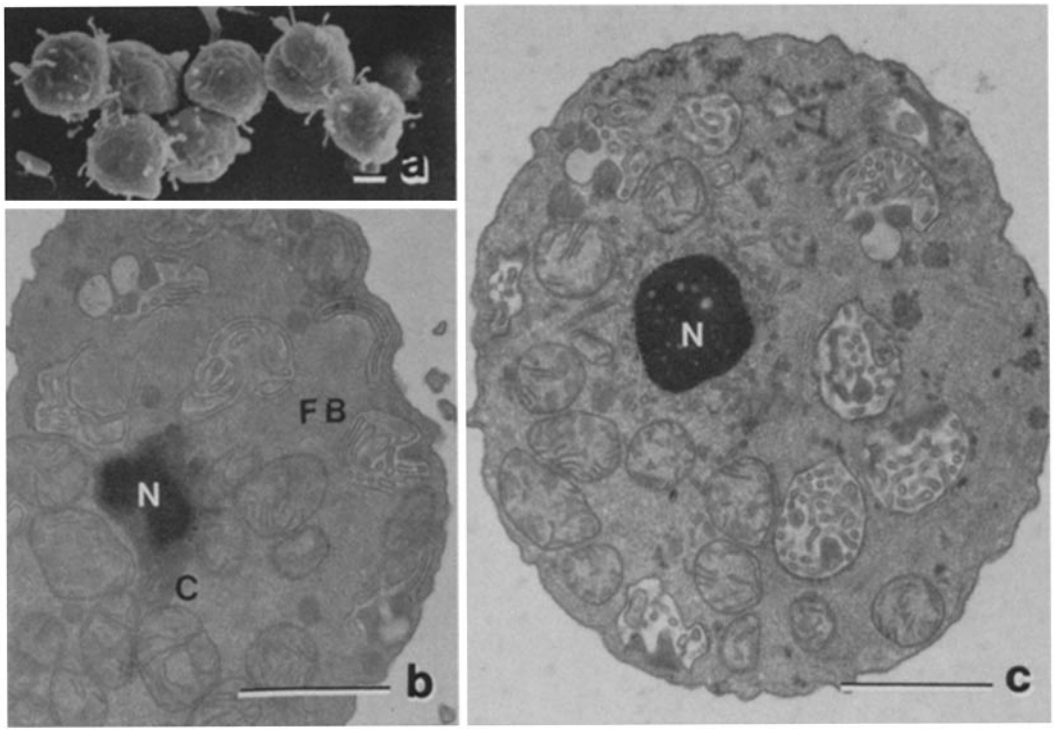

FIGURE 10 *fer-2* development. *a*, SEM of spermatids with thin and sparse microspikes. × 3,600. *b*, immature spermatid just after budding, before fibrous body (*FB*) disassembly. The perinuclear halo is present and surrounds the centriole (*C*). × 20,000. *c*, spermatid with large tubules in the perinuclear region. × 20,000. Bar, 1 μm.

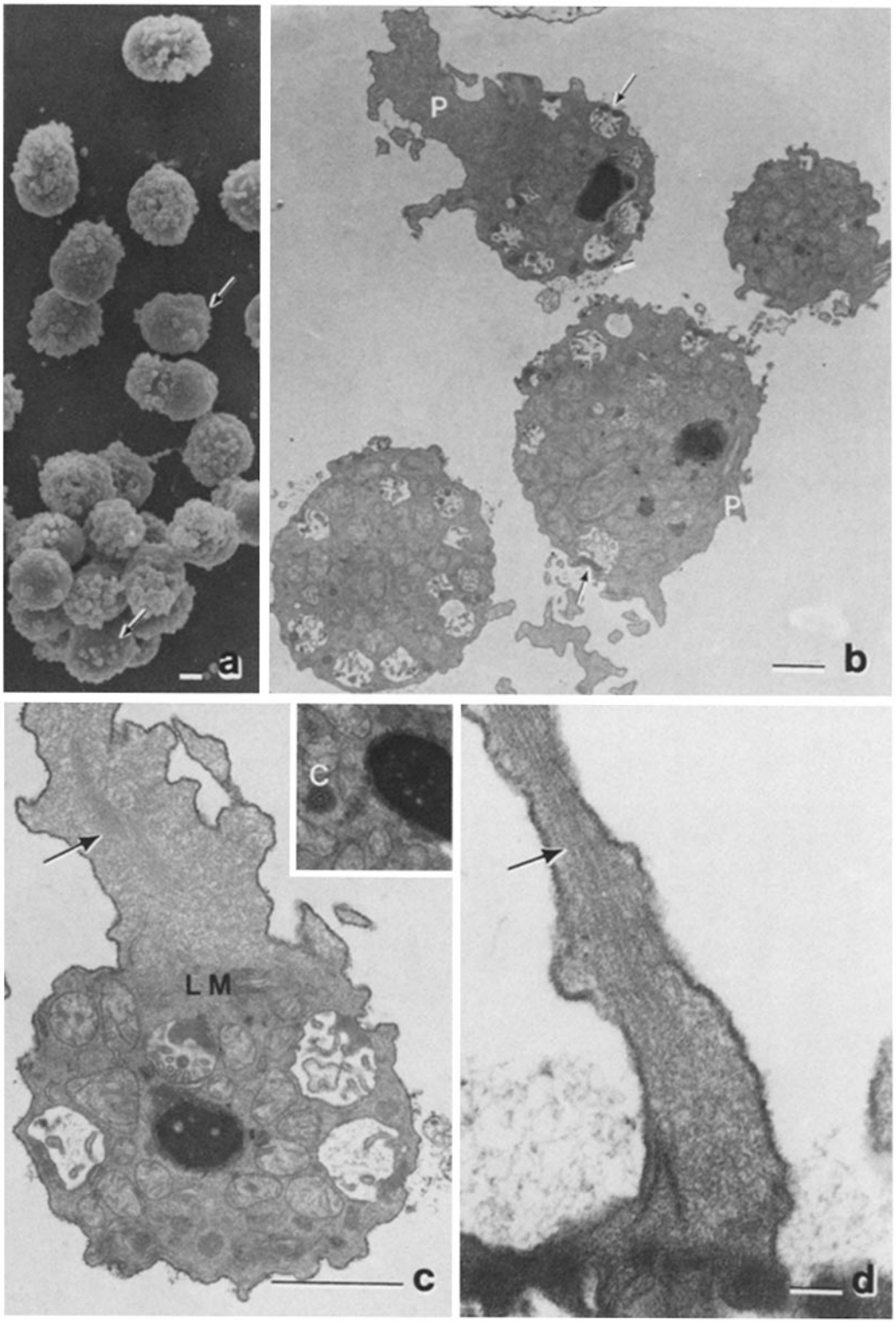

FIGURE 11 *fer-3* spermatozoa. *a*, SEM of a cluster of spermatozoa. Many look normal, but others (arrows) have short pseudopods. × 3,600. Bar, 1 μm. *b*, TEM of a field of aberrant spermatozoa. Arrows show fused MOs, others are seen in *c* and *d*. × 8,200. *c*, spermatozoon with filaments in pseudopod (arrow). × 20,000. *Inset* shows displaced centriole. × 20,000. *e*, filaments in a thin pseudopodial spike. × 80,000. *a–c*: bars, 1 μm; *d*: bar, 0.1 μm.

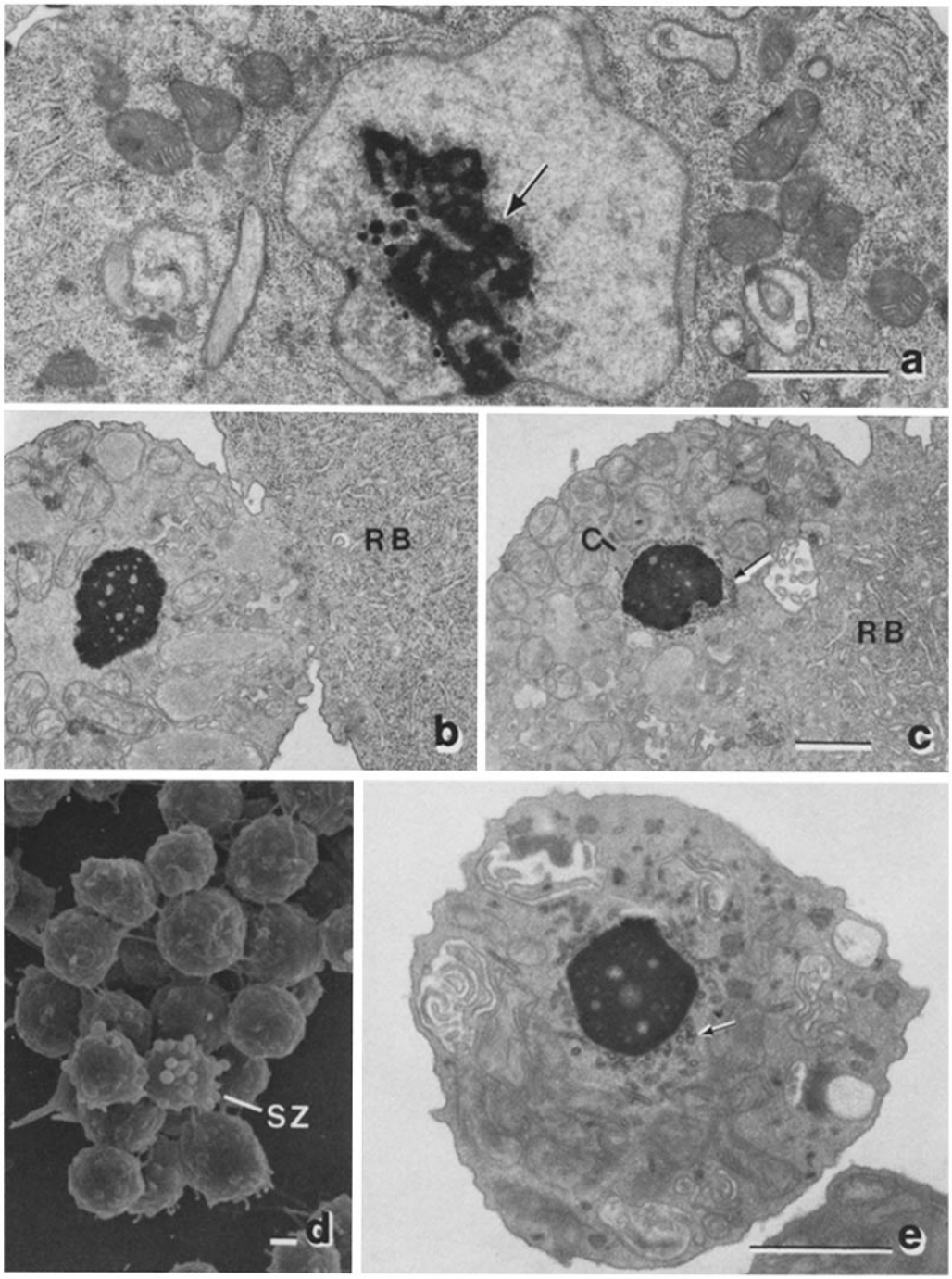

FIGURE 12 *fer-3* development. *a*, spermatocyte showing abnormal nucleolar condensation (arrow). × 20,000. *b*, normal looking immature spermatid budding from the residual body (*RB*). × 20,000. *c*, abnormal immature spermatid with ribosomes remaining around the nucleus (arrow), which also has a centriole (*C*). × 20,000. *d*, SEM of a cluster of spermatids and one spermatozoon (*SZ*). Spermatids have irregular shape and few microvilli. × 3,600. *e*, spermatid with large tubules (arrow) around nucleus. × 20,000. Bars, 1 μm.

Examination of the development of *fer-5* males sperm shows that spermatocytogenesis is normal and the separation from residual bodies is normal. The perinuclear halo is normal and includes the centriole; however, the laminar membranes appear much more extensive in *fer-5* spermatids than in wild-type (Fig. 15 *a*).

fer-6: *fer-6* spermatozoa are abnormal when examined by scanning EM (Fig. 16 *a*).They often have a skewered appearance and the pseudopods are spiky and aberrant. Most sperm from mated males do not have pseudopods at all. There are more crystalline inclusions than found in wild type (Fig. 16 *c*). MO fusions do occur in the rare spermatozoa (Fig. 16 *c* and *d*).

fer-6 mutant sperm appear to develop normally up to the budding of the spermatid (Fig. 17 *a*). When the spermatid buds, however, the fibrous bodies fail to disassemble. The MO membrane pulls away normally and folds into the normal compact MO, but the fibrous bodies remain intact (Fig. 17 *c* and *d*) even in spermatozoa (Fig. 16 *d*). The perinuclear halo is normal in

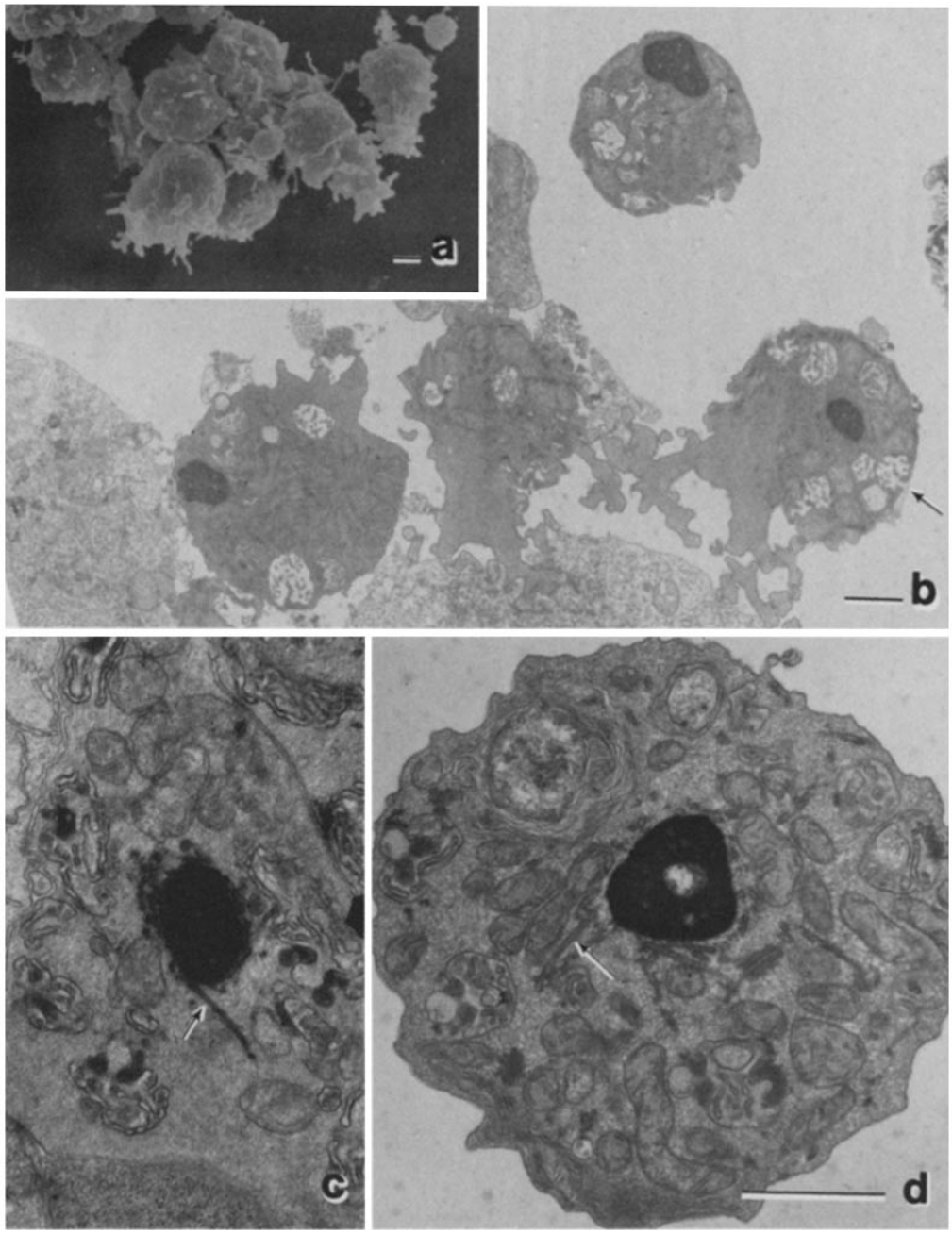

FIGURE 13 *fer-4*. *a*, SEM of a cluster of spermatozoa with abnormal pseudopodial projections. × 3,600. *b*, TEM of a field of spermatozoa with irregular pseudopods (P) and normal MO fusions (arrow). × 8,200. *c*, developing spermatid before budding with large tubules (arrow) already radiating from its nuclear region. × 20,000. *d*, spermatid with many large tubules (arrow) around its nucleus. × 20,000. Bars, 1 μm.

fer-6 spermatids and spermatozoa and includes the centriole.

DISCUSSION

The electron microscope examinations of sperm development reported here and previously (30, 38) enable one to describe the morphogenesis of the sperm as a series of individual morphogenetic events. In normal development these follow the precise sequence indicated in Fig. 5. There are events associated with the nucleus: condensation of chromosomes, spindle formation, nuclear membrane breakdown, chromatin segregation, reformation of the nuclear membrane, segregation of secondary nuclei, further condensation of the chromatin, and formation of the perinuclear halo. Events in the cytoplasm include: the segregation of organelles, the accumulation of ribosomes and the Golgi apparatus and the endoplasmic reticulum in the residual body, the formation of the membrane separating the spermatid from the residual body, the formation of tubular elements and laminar membranes, and the final rearrangements of organelles during spermiogenesis. The MO–fibrous body complex initially forms in the Golgi apparatus and increases in size; then its membrane separate from the fibrous body; the fibers disassemble (apparently distributing to the cytoplasm); the MO moves to abut the plasma membrane; and, finally, it fuses to release its contents. The surface membrane

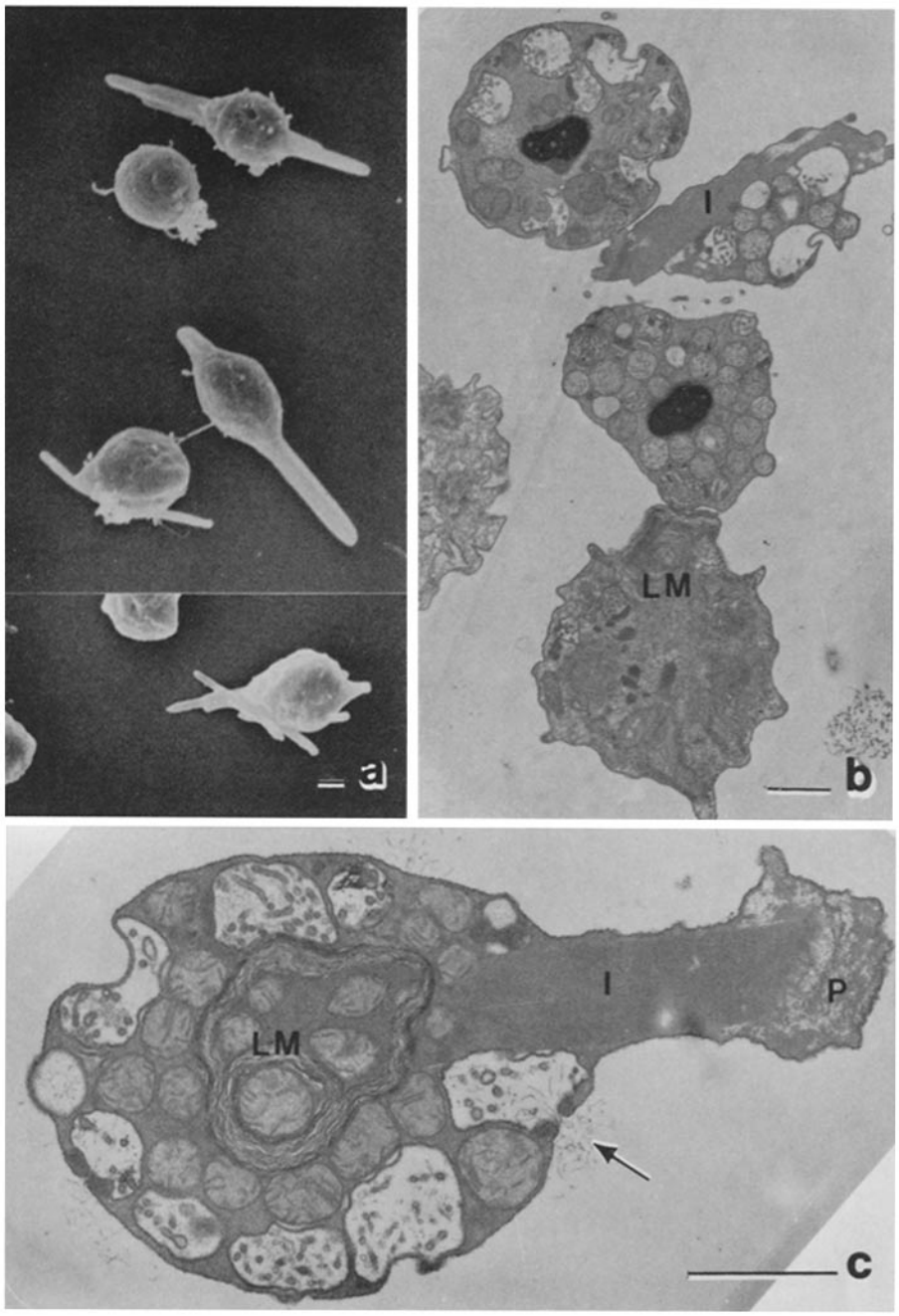

FIGURE 14 *fer-5*. *a*, SEM of abnormal sperm, probably all spermatids. × 3,600. *b*, TEM of a field showing spermatids with irregular shapes and cytoplasmic inclusions (*I*) and extensive laminar membranes (*LM*). *c*, a rare spermatozoon with cytoplasmic inclusion (*I*), filaments in the pseudopod (*P*), and fused MO (arrow). × 20,000. Bars, 1 μm.

also goes through a series of discrete changes: formation of the membrane separating the spermatid from the residual body, formation of microspikes, rearrangement of microspikes to the point of pseudopod extension, formation of the pseudopod, and movement of the pseudopod membrane.

These individual events must be specified genetically. The timing and sequence for each of them must be established and coordinated together to generate the final cell accurately. The small number of aberrant sperm, and the fact that nearly every sperm transferred fertilizes an egg (35), attests to the reliability and accuracy by which this process is achieved.

The analysis of mutant phenotypes reported here represents the beginning of an attempt to understand the genetic control of this precise process of spermatozoan morphogenesis. The mutant strains described here are apparently normal in phenotype except for their sterility, so they presumably identify genes that must function in sperm development but that are not essential for other cells (3). That mutations in such genes commonly alter morphology shows that many of the sperm-specific gene products must participate in the generation of the sperm's distinct morphology. Fig. 18 summarizes the development of morphological defects in these mutants. Except for *fer-3*, the mutant defects first become apparent late in sperm development during the maturation of the spermatid or the formation of the spermatozoa. This is when the majority of sperm-specific gene products would be needed, because it is

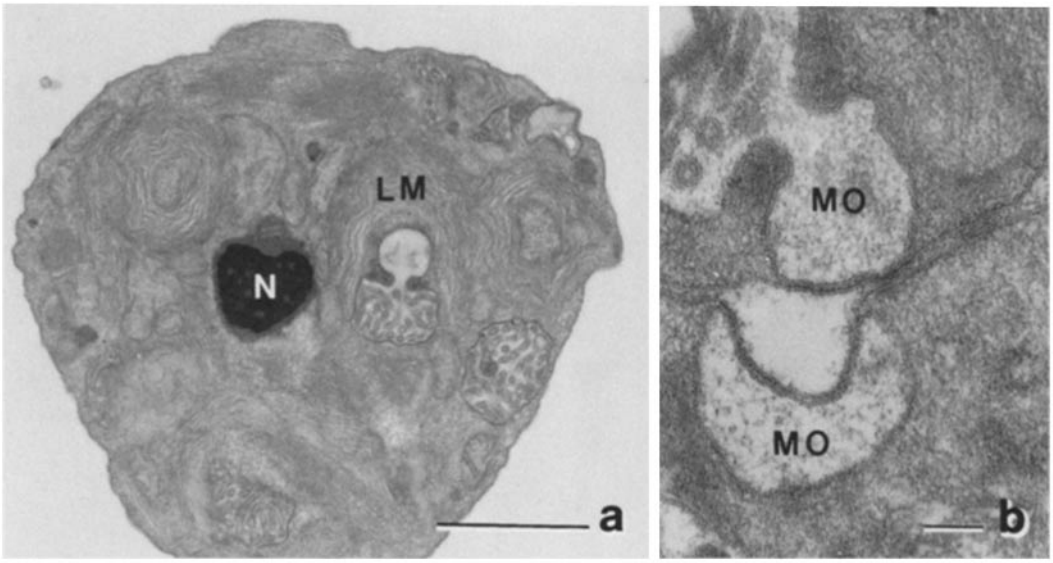

FIGURE 15 *fer-5* development. *a*, spermatid with extensive elaboration of laminar membranes (*LM*). Nucleus (*N*) has normal perinuclear cloud and centriole. × 20,000. Bar, 1 μm. *b*, MOs against plasma membrane in a spermatid. × 80,000. Bar, 0.1 μm.

during its terminal differentiation that the spermatozoon acquires its specializations.

The phenotype of *fer-1* mutant sperm shows that MO fusion is not necessary for the acquisition of cell asymmetry and the extension of a motile (though short) pseudopod. In addition, the phenotype of the majority of *fer-2* sperm, fused MOs with no pseudopod, shows that MO fusion is not sufficient for pseudopod formation. Therefore, these two mutants reveal that MO fusion and pseudopod formation are largely independent morphogenetic events.

Microspikes are normal on *fer-1* mutant spermatids and they disappear normally during spermiogenesis so this event is also independent of MO fusion. *fer-1* mutant sperm do not fully extend their pseudopod nor do they anchor to the walls of the spermatheca properly. In spite of this, they retain the ability to activate oocytes when they contact them (35). It is unlikely that MO fusion is absolutely necessary for a sperm to be fertile because *fer-1(24)* hermaphrodites produce 5–15 progeny and both *fer-1(hc1)* and *fer-1(hc24)* males produce some progeny during mating (3). Yet, in more than 1,000 spermatozoa examined, no MO fusions have been detected. Thus, it seems likely that the slight fertility of these mutants is not due to a few spermatozoa with fused MOs but probably reflects the ability of sperm with unfused MOs to fertilize eggs occasionally.

During normal development, the double membrane surrounding the fibrous bodies is infolded to form the mature MO at the same time that the fibers disappear. In *fer-6* mutant sperm, the MO membrane pulls away from the fibrous bodies normally to form the invaginated MO, but the fibrous bodies fail to disassemble. This shows that something must be holding the fibers together in addition to their enclosure by the MO membrane. It is not known why so few spermatids fail to become spermatozoa in this strain. Perhaps the disassembly of the fibrous elements is necessary for the cytoplasm to respond to the signal for activation.

The relationship between the phenotypes of *fer-2*, *fer-3*, and *fer-4* mutants is more complicated. In each of them, the perinuclear halo is altered and large tubules accumulate in its place. This occurs earliest in the development of *fer-4* sperm, before the normal time of perinuclear halo formation, and latest in *fer-2* sperm, after the apparent initial formation of a normal halo. In addition, the pseudopods are defective in *fer-2* and *fer-4* spermatozoa. It is not known whether the pseudopod defect is a result of the earlier defect in the perinuclear halo or whether both are the independent consequence of some other more general defect. In either case, the observation that MO fusion proceeds in these mutants says that the perinuclear halo is not required for MO localization or fusion. The formation of normal pseudopods in many *fer-3* spermatozoa also shows that a normal perinuclear region is not necessary for pseudopod formation.

The absence of large tubules or a perinuclear halo defect in any of the sperm in an *hc4/+* heterozygote shows that the presence of these structures cannot be the only cause of the *fer-4* mutant sperms' infertility. It may be that the presence of the wild-type allele during the diploid stages of spermatogenesis is sufficient to correct the perinuclear halo defect but not sufficient to restore fertility to all mutation bearing sperm.

The nature of the large tubules in *fer-2*, *fer-3*, and *fer-4* is unknown. Their diameter of ~50 nm is unlike that of any common tubular elements. They are larger than any of the aberrant "macrotubules" that tubulin can form (15). It may be that they represent an aberrant polymerized form of some protein present in the sperm. The normal perinuclear halo contains RNA, most likely in some ribonucleoprotein complex (Fig. 3). Because the large tubules appear to replace the perinuclear halo, they may be aberrant polymerized forms of ribonucleoprotein particles.

Aberrant polymerized structures accumulate during bacteriophage assembly when certain gene products are defective (reviewed in references 4, 39). These gene products can either be the major component of the aberrant structure, or they can be the minor components that interact with the major structural subunits. There is the further possibility that the aberrant formation of large tubules in the sperm could be sensitive to some general parameter of cell physiology such as ion composition or pH which could be altered by the *fer* mutations.

It is intriguing that *fer-2*, *fer-3*, and *fer-4* are the only *fer* mutants studied so far that produce an increase in defective embryos (3). This means that in the rare instances when

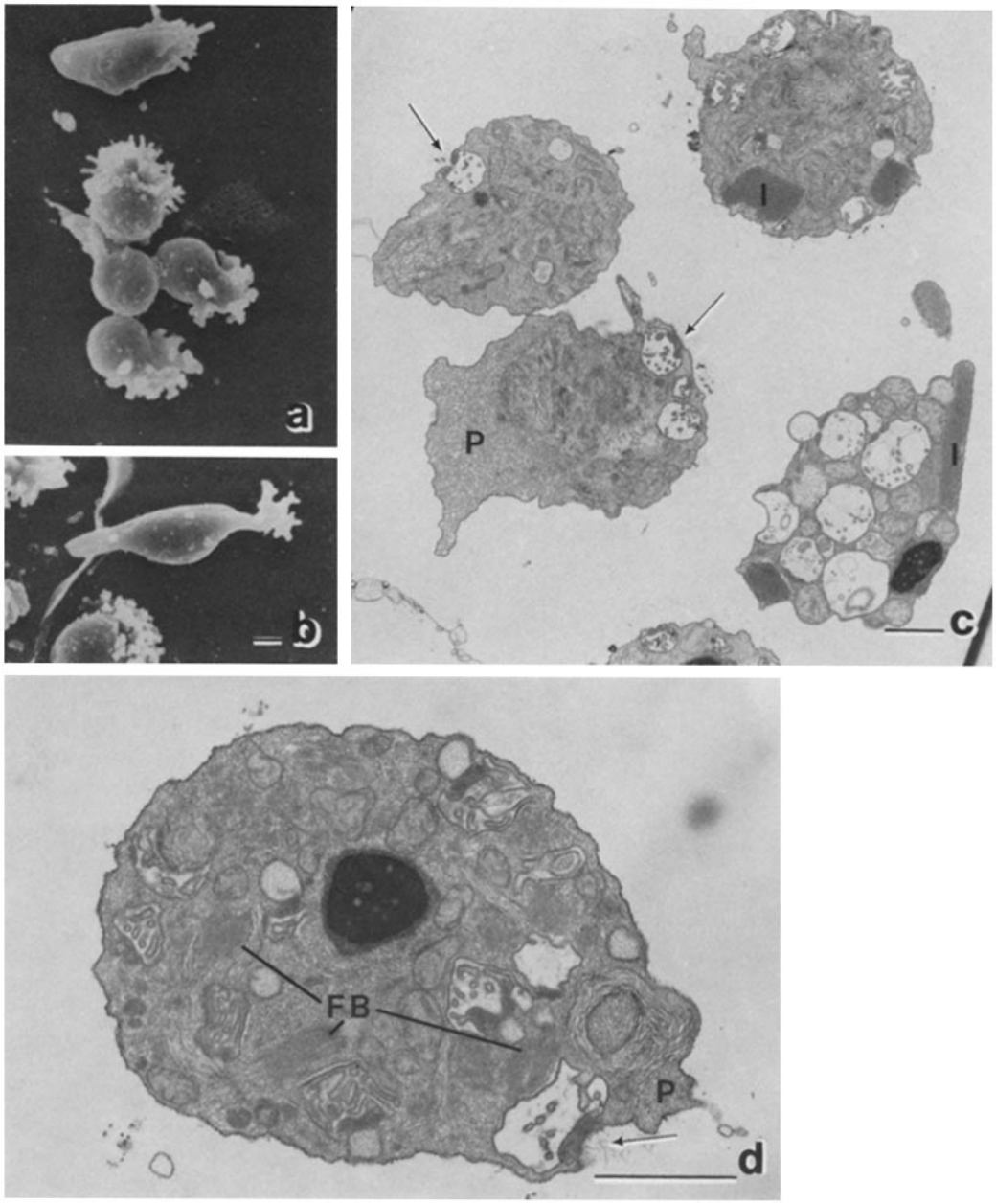

FIGURE 16 *fer-6* spermatozoa. *a* and *b*, SEM of spermatozoa with abnormal pseudopods. × 3,600. *c*, TEM of three spermatozoa and a spermatid (lower right). Several crystalline inclusions (*I*) are shown. × 8,200. *d*, spermatozoon with fibrous bodies (*FB*), one fused MO (arrow) and only a rudimentary pseudopod (*P*). × 20,000. Bars, 1 μm.

defective sperm do succeed in fertilizing an egg, the subsequent embryo is often defective. Because the perinuclear halo is the common defect in these three mutants, this defect might be the cause of the defective embryos. This would be consistent with the possibility that the normal perinuclear region could be contributing rRNA for support of embryonic development as in the parasitic nematode *Ascaris* (23).

The observation that the spermatozoa of all six of the *fer* mutants described have a discreet set of morphological defects shows that several of the events in sperm morphogenesis occur independently of each other. These include perinuclear halo formation, MO fusion, microspike rearrangement, and pseudopod formation. In the wild type, these events occur in a strict sequence. The mutant phenotypes show that this sequence cannot arise from a single pathway of morphogenesis in which each step is dependent on the previous steps. Instead, there must be multiple pathways of assembly, each leading to separate parts of the cell, as is found in the assembly of bacteriophage (11, reviewed in reference 39). Thus the principle of subassembly of components applies to these cells as well as viruses.

The recognition of separate pathways of assembly within the sperm comes from observing which morphogenetic events still proceed normally in a cell that has a visible defect. As discussed above, it is more difficult to interpret the relation between the multiple events which do not proceed normally in a defective cell. All of the mutations examined cause more than one defect in the spermatozoon, that is, they are pleiotropic. In analogy to mutants that affect more than one cell type in a whole organism (18), such pleiotropy could arise either because pathways of

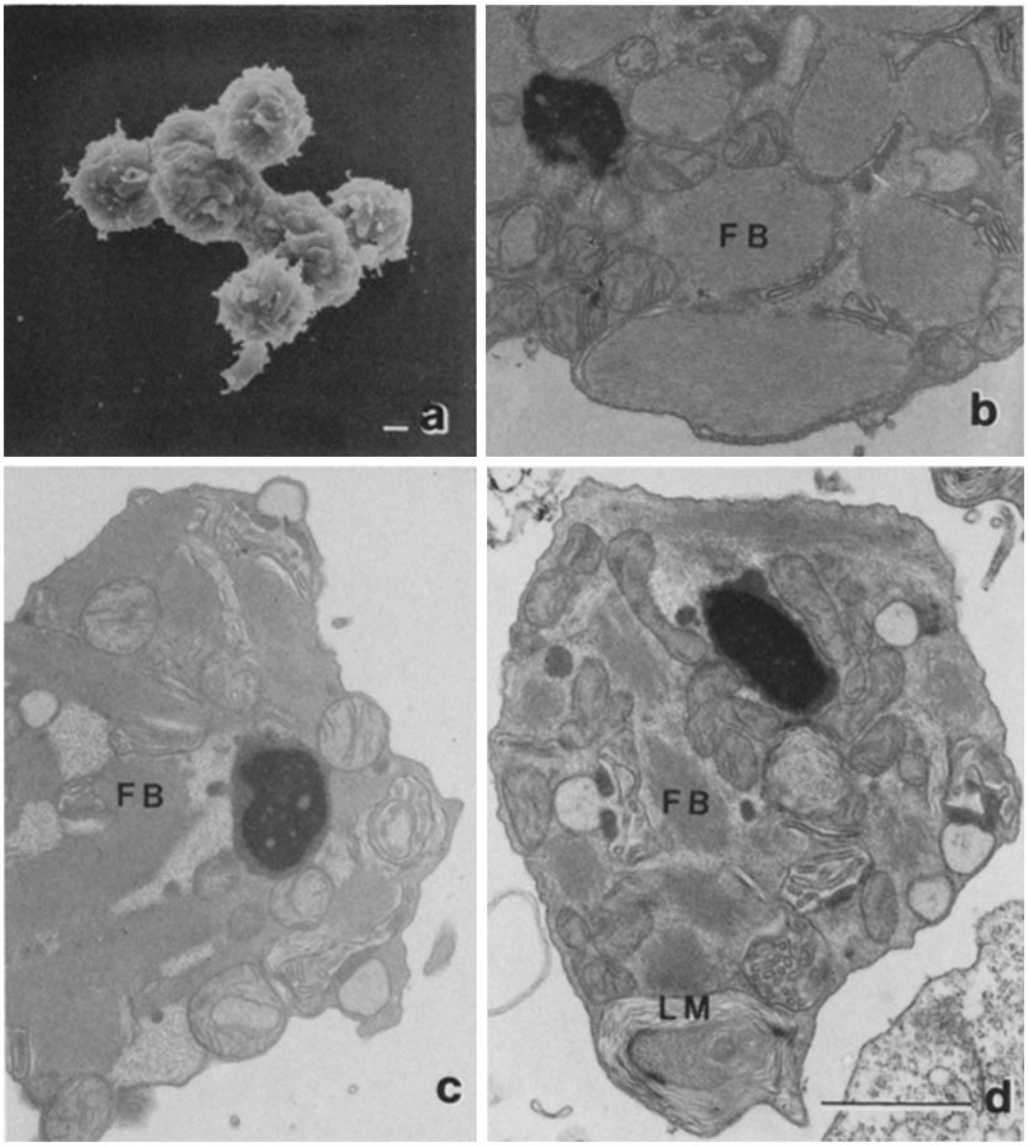

FIGURE 17 *fer-6* development. *a*, SEM of budding spermatid. × 3,600. *b*, normal lxoking fibrous bodies (*FB*) still surrounded by MO membrane in a budding spermatid. × 20,000. *c*, spermatid just after budding. The fibrous body fails to dissociate as the MO matures and pulls its membranes away. × 20,000. *d*, spermatid with mature MOs and undissociated fibrous bodies. × 20,000. Bars, 1 μm.

assembly are dependent on each other so the first visible defect causes the subsequent defects (relational pleiotropy) or because separate pathways of assembly require the same gene product (mosaic pleiotropy). We cannot resolve these alternatives until we have additional alleles of the mutant genes and know the identity of the mutated gene products.

Because all the mutations studied here are temperature-sensitive, we have previously determined the interval during sperm development that is temperature-sensitive for sterility (the temperature-sensitive period, TSP) (3). The TSP can be only roughly correlated with specific events in sperm development because spermatocytogenesis and spermiogenesis proceed simultaneously. In addition, it is not known whether the TSP represents the time a gene product is being synthesized or the time it is being utilized. Nonetheless, comparison of the TSP and the time of appearance of morphological defects reveals some consistency. The mutants in *fer-2*, *fer-3*, and *fer-4* all show TSPs that begin with early spermatogenesis and continue throughout as if they represent genes that are expressed and needed throughout sperm development. These mutants show the earliest morphological defects. *fer-5* and *fer-6* show a TSP starting somewhat later and their morphological defect also appears later. The TSP of *fer-1* also starts later and terminates before the accumulation of most of the mature spermatozoa in the hermaphrodite. This shows that the *fer-1* gene product is made or needed before the eventual expression of its morphological defect.

One puzzling aspect of the development of *C. elegans* sperm, as well as that of the related *Rhabditis pellio* and *Panagrellus*, is the appearance and disappearance of the fibrous bodies (5, 32, 38). These bodies arise from the endoplasmic reticulum and Golgi apparatus during spermatogenesis. They become bounded by double membranes that eventually become the MO. At the time of spermatid budding, the fibrous bodies are a dominant organelle in the cell, occupying 35% of its volume (S. Ward, unpublished observations). Yet shortly after bud-

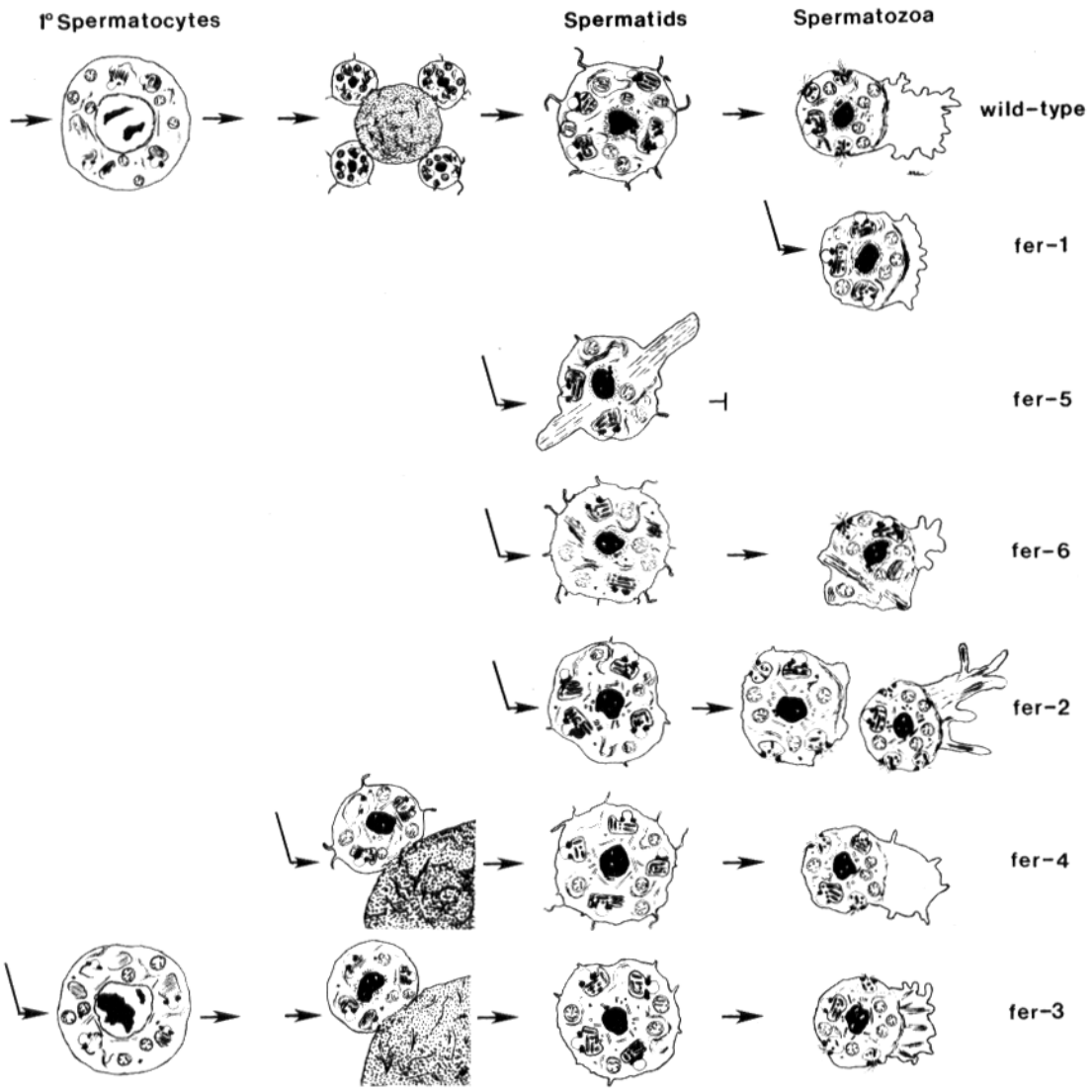

FIGURE 18 Summary of the development of morphological defects in *fer* mutant sperm. Angled arrows show where mutant sperm development becomes altered from wild type.

ding, their fibers disappear from the spermatid.

When purified sperm are disrupted with SDS and electrophoresed on SDS PAGE, one dominant protein is found with an apparent molecular weight of 15,000. This protein makes up 15–20% of the total sperm protein and has been designated the major sperm protein (MSP) (25, 29). It is not a nuclear protein and is readily released into the soluble fraction by cell lysis (25; S. Ward, unpublished observations). Because of its abundance, this protein is an obvious candidate for the contents of the fibrous bodies (38).

In the mature spermatozoon, the granular cytoplasm of the pseudopod represents nearly half of the volume (S. Ward, unpublished observations) and it is reasonable to guess that the MSP makes up the contents of the pseudopod as well. Support for the relation between the fibrous body contents and the pseudopod comes from examination of *fer-3* mutant pseudopods. These pseudopods often have a filamentous core with filaments the same width as those of the fibrous body filaments, suggesting that they may be made of the same subunit. Because the fibers in the *fer-3* pseudopod appear amidst the granular material it is likely that they arise from it and that the pseudopod and the fibrous bodies have similar composition. The MSP is a logical candidate for the structural component.

In *fer-5* and *fer-6*, a substantial fraction of the sperm have crystalline inclusions. These are similar to the inclusions seen in old wild-type sperm. Crystalline inclusions are usually found in cells that have one dominant protein that crystallizes due to its high local concentration (e.g. 12). If this is the case here, then the crystalline inclusions are likely to be made up of the MSP also. The observation that they are more abundant in *fer-5* and *fer-6* mutant sperm could be because these defective sperm resemble old wild-type cells that are dying and this causes the MSP to crystallize within them or these genes could affect the MSP directly as suggested by the failure of fibrous bodies to disassemble in *fer-6*.

If the above interpretations are correct, then the fibrous body filaments, the granular pseudopod contents, and the crystalline inclusions would each represent a different state of polymerization of the major sperm protein. Preliminary experiments using anti-MSP antiserum to localize the MSP support this interpretation (S. Ward and M. Klass, manuscript in preparation).

The results reported here show that the complexities of cellular morphogenesis can be dissected genetically to reveal individual pathways of assembly. Analysis of the small set of mutants reported here does not identify all of these pathways nor reveal their interconnections. The ease of isolation of sperm defective mutants, the ability to carry out sperm development *in vitro* and the availability of sperm in sufficient quantities for biochemical analysis encourages the hope that further analysis of these and other nematode sperm defective mutants will lead to a better understanding of the genetic control of morphological differentiation.

We thank Gail Korman and William Duncan for preparation of sections. We have benefitted from many discussions and critical reading of the manuscript by our colleagues Ken Muller, Tom Roberts, and Dan Burke. We thank Susan Satchell for skillful preparation of the manuscript.

This research was supported by grants GM25243 and GM22203 to S. Ward and by the Carnegie Institution of Washington.

Received for publication 10 November 1980, and in revised form 8 May 1981.

REFERENCES

1. Abbas, M., and G. D. Cain. 1979. *In vitro* activation and behavior of the amoeboid sperm of *Ascaris suum* (Nematoda). *Cell Tissue Res.* 200:273–284.
2. Albertson, D. G., J. E. Sulston, and J. G. White. 1978. Cell cycling and DNA replication in a mutant blocked in cell division in the nematode *Caenorhabditis elegans*. *Dev. Biol.* 63: 165–178.
3. Argon, Y., and S. Ward. 1980. *Caenorhabditis elegans* fertilization-defective mutants that have defective sperm. *Genetics.* 96:413–433.
4. Atabekov, J. G. 1977. Defective and satellite plant viruses. *In* Comprehensive Virology, H. Fraenkel-Conrat and R. R. Wagner, editors. Plenum Press, New York. 11:143–200.
5. Beams, H. W., and S. S. Sekhon. 1972. Cytodifferentiation during spermiogenesis in *Rhabditis pellio*. *J. Ultrastruct. Res.* 38:511–527.
6. Bernhard, W. 1969. A new staining procedure for electron microscopical cytology. *J. Ultrastruct. Res.* 27:250–265.
7. Brenner, S. 1974. The genetics of *Caenorhabditis elegants*. *Genetics.* 77:71–94.
8. Burghardt, R. C., and W. E. Foor. 1978. Membrane fusion during spermiogenesis in *Ascaris*. *J. Ulstrastruct. Res.* 62:190–202.
9. Chalfie, M., and J. N. Thomson. 1979. Organization of neuronal microtubules in the nematode *Caenorhabditis elegans*. *J. Cell Biol.* 82:278–289.
10. Clark, W. H., R. L. Moretti, and W. W. Thomson. 1972. Histochemical and ultracytochemical studies of the spermatids and sperm of *Ascaris lumbricoides* var. *suum*. *Biol. Reprod.* 7:145–159.
11. Edgar, R. S., and W. B. Wood. 1966. Morphogenesis of bacteriophage T4 in extracts of mutant-infected cells. *Proc. Natl. Acad. Sci. U. S. A.* 55:498–505.
12. Fawcett, D. W. 1966. An Atlas of Fine Structure: The Cell. Saunders, New York.
13. Fawcett, D. W. 1975. The mammalian spermatozoon. *Dev. Biol.* 44:394–436.
14. Foor, W. E. 1970. Spermatozoan morphology and zygote formation in nematodes. *Biol. Reprod.* 2(suppl.):177–202.
15. Fujiwara, K., and L. G. Tilney. 1975. Structural analysis of the microtubule and its polymorphic forms. *Ann. N. Y. Acad. Sci.* 253:27–50.
16. Goldstein, P. 1977. Spermatogenesis and spermiogenesis in *Ascaris lumbricoides* var. *suum*. *J. Morphol.* 154:317–338.
17. Goldstein, P., and A. C. Triantaphyllou. 1980. The ultrastructure of sperm development in the plant-parasitic nematode *Meloidogyne hapla*. *J. Ultrastruct. Res.* 71:143–153.
18. Gruneberg, H. 1973. The pathology of development. *In* A Study of Inherited Skeletal Disorders in Animals. John Wiley and Sons, Inc., New York.
19. Hirsh, D., and R. Vanderslice. 1976. Temperature-sensitive developmental mutants of *Caenorhabditis elegans*. *Dev. Biol.* 49:220–235.
20. Hodgkin, J., H. R. Horvitz, and S. Brenner. 1979. Nondisjunction mutants of the nematode *Caenorhabditis elegans*. *Genetics.* 91:67–94.
21. Horvitz, H. R., S. Brenner, J. Hodgkin, and R. K. Herman. 1979. A uniform genetic nomenclature for the nematode *Caenorhabditis elegans*. *Mol. Gen. Genet.* 175:129–133.
22. Karnovsky, M. J. 1965. A formaldehyde-glutaraldehyde fixative of high osmolarity for use in electron microscopy. *J. Cell Biol.* 27(2, Pt. 2):137*a* (Abstr.).
23. Kaulenas, M. S., and D. Fairbairn. 1968. RNA metabolism of fertilized *Ascaris lumbricoides* eggs during uterine development. *Exp. Cell Res.* 52:233–251.
24. Klass, M., N. Wolf, and D. Hirsh. 1976. Development of the male reproductive system and sexual transformation in the nematode *Caenorhabditis elegans*. *Dev. Biol.* 52:1–18.
25. Klass, M., and D. Hirsh. 1981. Sperm isolation and biochemical analysis of the major sperm protein from *Caenorhabditis elegans*. *Dev. Biol.* In press.
26. McLaren, D. J. 1973. The structure and development of the spermatozoon of *Dipetalonema viteae* (Nematoda: Filaroidea). *Parasitology.* 66:447–463.
27. Neill, B. W., and K. A. Wright. 1973. Spermatogenesis in the hologonic testis of the trichuroid nematode, *Capillaria hepatica* (Bancroft, 1983). *J. Ulstrastruct. Res.* 44:210–234.
28. Nelson, G. A. 1979. Nematode sperm motility. Carnegie Institution Year Book, Carnegie Institution of Washington. 78:62–66.
29. Nelson, G. A., T. M. Roberts, and S. Ward. 1981. *C. elegans* spermatozoan locomotion: amoeboid movement with almost no actin. *J. Cell Biol.* In press.
30. Nelson, G. A., and S. Ward. 1980a. Vesicle fusion, pseudopod extension and amoeboid motility are induced in nematode spermatids by the ionophore monensin. *Cell.* 19:457–464.
31. O'Brien, T. P., and M. E. McCully. 1969. Plant Structure and Development. A Pictorial and Physiological Approach. Collier-Macmillan Canada, Ltd., Toronto.
32. Pasternak, J., and M. R. Samoiloff. 1972. Cytoplasmic organelles present during spermatogenesis in the free-living nematode *Panagrellus silusiae*. *Can. J. Zool.* 50:147–151.
33. Phillips, D. M. 1974. Spermiogenesis. Academic Press, Inc., New York.
34. Riddle, D. L. 1978. The genetics of development and behavior in *Caenorhabditis elegans*. *J. Nematol.* 10:1–16.
35. Ward, S., and J. S. Carrel. 1979. Fertilization and sperm competition in the nematode *Caenorhabditis elegans*. *Dev. Biol.* 73:304–321.
36. Ward, S., and J. Miwa. 1978. Characterization of temperature-sensitive fertilization-defective mutants of the nematode *Caenorhabditis elegans*. *Genetics.* 88:285–303.
37. Ward, S., J. N. Thomson, J. G. White, and S. Brenner. 1975. Electron microscopical reconstruction of the anterior sensory anatomy of the nematode *Caenorhabditis elegans*. *J. Comp. Neurol.* 160:313–338.
38. Wolf, N., D. Hirsh, and J. R. McIntosh. 1978. Spermatogenesis in males of the free living nematode *Caenorhabditis elegans*. *J. Ultrastruct. Res.* 63:155–169.
39. Wood, W. B., and J. King. 1979. Genetic control of complex bacteriophage assembly. *In* Comprehensive Virology. H. Fraenkel-Conrat and R. R. Wagner, editors. Plenum Press, Inc., New York. 13:581–634.
40. Yamada, E. 1957. The fine structure of the megakaryocyte in the mouse spleen. *Acta Anat.* 29:267–290.